Mechanical Properties of Tetra-Polyethylene and Tetra-Polyethylene Oxide Diamond Networks via Molecular Dynamics Simulations

A Thesis

Presented to the Faculty of the Graduate School

of Cornell University

in Partial Fulfillment of the Requirements for the Degree of

Master of Science

by Endian Wang

February 2016

ABSTRACT

The tensile response to uniaxial deformation of polyethylene-based (Tetra-PE) and polyethylene glycol-based (Tetra-PEG) networks of various strand lengths with idealized diamond connectivity have been studied via atomistic molecular dynamics simulations. Tetra-PE and Tetra-PEG diamond networks with the same strand length show comparable maximum extensibility but the Young's moduli and tensile strength of the former are significantly lower than those of the latter, consistent with stronger intersegmental attractions in the amorphous Tetra-PEG networks. The stress-strain curves show that the stress in short-stranded networks increased rapidly and monotonically with strain while for long-stranded networks it increased very little at small strain, in a non-monotonic fashion at intermediate strains, and then very sharply as the limit of extensibility was approached. Spontaneous partial crystallization of a long-stranded Tetra-PE diamond network under supercooling was demonstrated, and the resulting system was used to: (1) Estimate its melting point as the temperature where any crystalline material disappeared abruptly, and (2) show that the presence of crystalline material in the undeformed state leads to higher stress responses upon deformation compared to amorphous samples, a result consistent with experimental observations. The spontaneous crystallization of Tetra-PEG networks at large supercooling was unsuccessful due to the slow motions of the network beads and the prohibitively long crystal nucleation times entailed.

BIOGRAPHICAL SKETCH

The author, Endian Wang, born in Fujian, China, attended his middle school and high school in Karamay, Xinjiang in the northwest of China after moved out from his hometown with his parents in 1999. After entering to Dalian University of Technology in 2007, he majored in process control in chemical engineering. In 2010, he exchanged to study chemical and bio-molecular engineering in University of Sydney, Australia. With the help from his undergraduate thesis adviser Prof. Tim Langrish, he coauthored with Dr. Debolina, published a research paper, entitled “Solid-phase crystallization of spray-dried glucose powders”, which awarded with John Brodie Medal. He graduated and received two bachelor degrees from these two universities in 2013. He obtained his Master of Engineering degree from Cornell University in 2014. He started his research under the supervision of Prof. Fernando Escobedo in the same year.

He studied and enjoyed sketching and oil painting during middle school and high school, and would like to continue painting in the near future.

ACKNOWLEDGEMENTS

I would like to first thank my thesis advisor, Prof. Fernando Escobedo. He has helped and encouraged me throughout the research, his support and wisdom led me to the right way. His enthusiasm for scientific research and teaching has greatly motivated me.

I also would like to thank my thesis committee advisor, Prof. Claude Cohen, who, although approaching his retirement, has come to my committee meeting and challenged me with out-of-expectation questions that reminded me of the gaps in my knowledge. He reviewed my thesis paper and kindly offered insightful comments.

I also would like to thank the current and former Escobedo group members, including Sushmit, Sai Pooja, Poornima, Vikram, Mohammed, Christ and Unmukt. Some of them shared their rich knowledge in simulation and software, and others expanded my exposure to wider topics and research techniques outside my own thesis topics.

I want to thank my parents. Without their unconditional love and sacrifice, I could have never been here today.

Last but not the least, I want to acknowledge the financial support from the NSF (National Science Foundation).

Table of Contents

1. INTRODUCTION

Branched and crosslinked polymers such as elastomers (rubbers), thermoplastics and organic and inorganic gels have played an increasingly important role not only in the traditional fields (i.e., textile, automotive and construction industries) [1], but also in more modern biomedical applications (i.e., contact lenses, drug delivery systems and artificial articular cartilage) [2]. The unique properties of polymer networks have stimulated extensive research to elucidate the connection between the microscopic structure and the elastic properties of the material. The chemistry and molecular weight of the precursor chains and the extent of interchain connectivity of these systems leads to materials with a tunable combination of liquid-like and solid-like properties [3], which has fueled a large and still growing number of practical applications in various fields.

It is known that the physical properties of crosslinked polymers are strongly dependent on the chemical structure and spatial homogeneity of the network [4]. Therefore, control of the network structure of crosslinked polymers has long been investigated by various methods in order to improve their thermophysical properties. Several approaches have been advanced in the quest for eliminating the inhomogenities in a polymer network. In particular, an idealized class of polymer networks of homogeneous and uniform structure denoted as “diamond networks” has been studied [5, 6] over the past two decades. In this “chemically” defect-free polymer network, the mean topological locations of its crosslinks correspond to those of a diamond lattice sites, with each network strand corresponding to the “bond” between such lattice sites [7]. This diamond polymer network has been studied not only in computer simulations [3, 8-11], but it appears to

have also been approximated by a synthetic approach [12] that uses the programmed self-assembly of molecular building blocks made of branched polyethylene glycol (PEG) moieties. By combining two symmetrical tetrahedron-like macromonomers of the same size, the resultant so-called Tetra-PEG gel is posited to be a fairly homogeneous diamond-like network [13], which has been shown to have a high mechanical strength comparable to human articular cartilage [14]. Its facile synthesis and high mechanical strength make Tetra-PEG a valuable candidate for many biomedical applications, such as drug delivery systems [15] and regenerative medicine [16].

While many studies have focused on the theoretical and experimental aspects of the diamond-like polymer networks, our understanding of such systems is still incomplete [8, 17-19]. In particular, there are no atomistic simulation studies that have explored how specific chain chemistries and interactions influence the mechanical properties of diamond networks. Although various simulation techniques have been used in order to model the polymer network of diamond-like connectivity, many of the results tend to be rather limited in scope. Escobedo and de Pablo [1] investigated the swelling behavior of such networks by using Mote Carlo simulations technique. Sugimura et al. [19] developed a network model using a worm-like chain (WLC) potential to evaluate the relationship between spatial inhomogenities and mechanical properties of Tetra-PEG diamond networks. Aguilera-Mercado et al. [8] studied the uniaxial tensile response of a diamond networks made up of semiflexible and block copolymer chains using coarse-grained models and showed that such systems can give rise to a novel saw-tooth shaped response associated with multiple ordering transitions. While these results have provided valuable insights into the microscopic origin of the network elastic behavior, both the coarse-grained model and the WLC-chain model may not accurately capture some of the important details about the molecular interactions that determine their structure and dynamics. As such,

those models are inherently inadequate to study processes where, e.g., crystal-to-amorphous phase transitions may occur. To the best of our knowledge, no atomistic simulation has been reported that employs realistic force-fields to probe the mechanical properties of perfect diamond networks, which could be compared with experimental observations on diamond-like networks.

It is well established that the mechanical behavior of polymers is closely coupled to their morphology, which in turn is determined by the conditions during processing [20]. A number of polymers have the ability to form crystalline materials at appropriate conditions. To explore the mechanical properties of the diamond network whose precursor chains are below or near their melting temperature, one can validly consider processing conditions where the undeformed sample generated has either (i) an amorphous structure or (ii) a (partially) crystalline structure. Although crystallization of polymers has been extensively investigated through various experimental techniques including optical microscopy, light scattering, X-ray scattering, and atomic force microscopy, the existing results from computer simulations are mainly concentrated on small linear n-alkane molecules [21-24] and polyethylene [25, 26]. The effects of crystal content on the strength of a polymer diamond network are yet unknown; moreover, it is unclear in such systems how chains would fold into crystal lamellae and how the crosslinks could affect the extent of crystallization.

This work aims at exploring the mechanical properties of homogeneous diamond networks of specific strand chemistries through molecular dynamics (MD) simulations. Among the many appealing chemistries, we have selected first n-alkanes as network strands since they have been extensively studied in the literature and are the building block of polyethylene and of other important polymers and oligomers [23]. Such networks will be referred to as Tetra-PE networks. The second chemistry selected is based on Poly(ethylene oxide) (PEO) as the network strands,

motivated by the many experimental studies of Tetra-PEG networks [12]. To study the influence of chain length (or degree of polymerization) on the mechanical properties of Tetra-PE and Tetra-PEG diamond networks, we perform uniaxial deformation simulations for systems of various strand lengths. For selected cases, we also explore the crystallization behavior of the network since the difference between the temperature of interest and the melting temperature has a significant effect on the proclivity of the networks to undergo strain-induced crystallization. Overall, this work attempts to quantify the effects of chain length and polymer morphology on the mechanical properties of atomistic models of polymer diamond networks made from simple but important monomers, and to provide insights into designs that could enhance such properties.

The remainder of this manuscript is organized as follows. In sections 2.1 and 2.2 we introduce the network system details and modeling protocols, while in section 2.3 we describe the force field potential adopted. In section 2.4 we describe the local order parameter used to characterize the crystal fraction of the Tetra-PE and Tetra-PEG systems. In section 3.1 we present the results for the crystallization of a selected Tetra-PE system and for uniaxial deformation of Tetra-PE systems of various chain lengths. In section 3.2 we discuss the effect of chain length of Tetra-PEG systems on (i) the proclivity to undergo strain-induced crystallization and (ii) the stress response to uniaxial deformation, including a comparison with experimental data of the Young's modulus. Finally, we give in section 4 some concluding remarks. Additional details on the simulations and results are given in a Supplementary Information (SI).

2. SIMULATION METHODOLOGY

2.1. Polymer Diamond Network Systems

2.1.1. Tetra-PE Diamond Network

A total of 7 Tetra-PE diamond network systems were built with degree of polymerization [or number of methylene ($-CH_2-$) groups on each network strand] n = 6, 12, 18, 30, 39, 75 and 100. Each network consisted of 8 units of diamond cell, so that 64 tetra-functional crosslinks and 128 chains in each system formed a cubic periodic structure. The n=100 system was simulated for studying the isothermal spontaneous crystallization process and the strain-induced crystallization. Due to its long chains, this system consisted of only 4 diamond cell units, 32 crosslinks and 64 strands (the initial dimensions of the simulation box along each axis are such that $L_x = L_y = 2 \times L_z$) and the uniaxial deformation was performed along the z axis.

2.1.2. Tetra-PEG Diamond Network

Consistent with the structure of the ideal network that could be achieved by the experiments with Tetra-gels [4, 12, 17-19], we created seven Tetra-PEG ideal diamond networks corresponding to different degrees of polymerization of the network strands. The network chains were made of poly(ethylene oxide) PEO oligomers; i.e., each end of a $-CH_2O-[CH_2CH_2O]_n-CH_2-$ chain was connected to a carbon atom functioning as a tetra-functional crosslink. The systems had degree of polymerization (the number of $-CH_2CH_2O-$ groups) n ranging from 1 to 40. The systems with n = 1, 3, 5, 9 and 12, contained eight units of diamond cell (64 tetra-functional crosslinks and 128 chains), while the systems with n = 24 and 40 contained only four diamond unit cells (32 crosslinks and 64 chains).

2.2. Simulation Protocols

All the simulations were performed using the molecular dynamics (MD) simulator LAMMPS [27]. The idealized diamond-like network was created with all crosslinks initially lying on the lattice points of a diamond lattice. Periodic boundary conditions were used in all directions of the orthorhombic simulation box. Each system was initially prepared using an isothermal isochoric NVT ensemble to randomize the coordinates of the molecules in the simulation box at 450 K for 1 ns at density of 0.5 $g \cdot cm^{-3}$, followed by equilibration in an isothermal isobaric NPT ensemble at 303.15 K and 1 atm using the Nosé-Hoover thermostat [28, 29] and Nosé-Hoover barostat for 2 ns or until converged values were observed (i.e., properties such as the system density and average bending angle reached plateau values). The damping and drag parameters for both barostat and thermostat were 100 and 0 respectively. The MD simulation was performed via the leapfrog algorithm using a time step of 1 fs.

To estimate the network melting point for the n=100 Tetra-PE, an amorphous system initially prepared at 303 K was equilibrated at 260 K and 1 atm in the NPT ensemble while allowing the nucleation and growth of crystalline material. The changes in crystal fraction over the simulation time were monitored through changes of a local order parameter (as defined in Subsection 2.4) for all beads in the system. After the total crystal fraction in the n=100 Tetra-PE system reached a plateau value, the system was taken as the initial configuration to perform NPT simulations at different temperatures from 280 K to 360 K. Using this technique (which has been used before with linear alkanes [21-23]), an upper bound for the melting point temperature was identified as the lowest temperature at which the solid melts completely into a liquid.

For uniaxial deformation simulations, the stress-strain curve can be obtained via either a strain-driven (at constant total volume) ensemble or a stress-driven ensemble. In the latter, a constant

pressure > 1 bar is applied in the deformation direction (z) while a pressure of 1 bar is applied along the orthogonal directions of the simulation box (where deformations are coupled so that the box cross section is always a square, i.e., $L_x = L_y$). We found that stress-strain curves obtained via either ensemble were almost indistinguishable as long as the density in the stress-driven simulations is consistent with the average density of the strain-driven simulations (see Fig. S1 in the SI for a relevant comparison). Although the stress-driven ensemble is a better representation of typical experimental conditions, the strain-driven ensemble (which assumes a material with a Poisson ratio = 0.5) is often favored in deformation simulations [30-32] as it allows for faster simulations (noting that, for a given strain, it corresponds to an isothermal isochoric or NVT ensemble). Hence, for the results reported hereon, only strain-driven or canonical (NVT) ensemble results are reported for the deformation of the Tetra-PE and Tetra-PEG diamond networks.

Each deformation simulation in the strain-driven NVT ensemble is conducted so that for any elongation along the strain axis the cross-section of the simulation box (perpendicular to the applied stress direction) was concertedly contracted. The instantaneous length of the simulation box parallel to the direction of applied tension is defined as:

$$L(t) = L_0(1 + \dot{r} \cdot t) \tag{1}$$

where $\dot{r}$ is the strain rate constant (in units of fs^{-1}), L_0 denotes the initial length of the simulation box prior to the application of tension and t is the elapsed time (in units of fs). The strain at each time step can be calculated as:

$$\varepsilon(t) = \frac{L(t) - L_0}{L_0} \tag{2}$$

During the deformation process, the pressure tensor components P_{xx} , P_{yy} and P_{zz} on each dimension of the simulation box were monitored every 2000 time steps, the net tension along the deformation direction (z axis) was calculated from [7, 19]:

$$\sigma_{zz} = \lambda\left(P_{zz} - \frac{P_{xx} + P_{yy}}{2} \right) \tag{3}$$

where a Poisson ratio λ = 0.5 was assumed (appropriate for incompressible rubberlike materials [7]). The stress values reported in the stress-strain plots are the averages of the instantaneous values taken over strain intervals of $\Delta\varepsilon$ = 0.05.

2.3. Force Field and Potential Model

2.3.1. Force Field Parameters for Tetra-PE Systems

The TraPPE- UA (United Atom) force field [33] was chosen for the MD simulation of the Tetra-PE system. It has been demonstrated that this transferable force field is computationally efficient for linear and branched alkanes, and can accurately predict a wide range of thermo-physical properties [34]. The TraPPE-UA force field employs pseudo-atoms for all CH_x groups ($0 \leq x \leq 4$). For our simulations, the non-bonded interactions for CH_2 united atom and the crosslinks carbon followed the simple pairwise-additive Lennard-Jones (LJ):

$$U_{nonbonded} = 4\varepsilon_{ij}\left[\left(\frac{\sigma_{ij}}{r_{ij}} \right)^{12} - \left(\frac{\sigma_{ij}}{r_{ij}} \right)^{6} \right], \quad r_{ij} < r_c \tag{4}$$

The pair-wise LJ diameter σ and the energy well depth ε parameter values are tabulated in Table S1 in the SI. The cutoff distance r_c is taken as 0.9 nm. All united atoms in these systems

have no partial change. The unlike LJ interactions are determined using Lorentz-Berthelot combining rules:

$$\sigma_{ij} = \frac{1}{2}\left(\sigma_{ii} + \sigma_{jj}\right) \quad and \quad \varepsilon_{ij} = \left(\varepsilon_{ii}\varepsilon_{jj}\right)^{\frac{1}{2}} \tag{5}$$

The standard TraPPE non-bonded potential is calculated for all intermolecular interactions involving pseudo-atoms separated by four or more bonds. All alkyl group and functional groups are typically treated as having fixed bond lengths in the TraPPE-UA force field. However, because LAMMPS limits the use of the SHAKE algorithm [35] to restrain the bond lengths [36], we adopt here a harmonic potential for the interaction between bonded pairs of united atoms:

$$U_{bond}\left(r\right) = \frac{k_r}{2}\left(r - r_0\right)^2 \tag{6}$$

For all bond types, the k_r constant is $1004.239\text{kJ} \cdot \text{mol}^{-1} \cdot \text{nm}^{-2}$ based on the PYS united atom force field described by Paul et al. [37], with equilibrium bond length [34, 38] $r_0\left(\text{CH}_\text{x} - \text{CH}_\text{y}\right)_{\text{x,y=2,3}} = 0.154\ \text{nm}$. Beads separated by two bonds forming the angle θ interact via a harmonic bending potential [33]:

$$U_{bend}\left(\theta\right) = \frac{k_\theta}{2}\left(\theta - \theta_0\right)^2 \tag{7}$$

The equilibrium angle $\theta_0 = 114°$ for $\text{CH}_2 - \text{CH}_2 - \text{CH}_2$, $\theta_0 = 109.47°$ for $\text{CH}_2 - \text{C} - \text{CH}_2$, the force constants $k_\theta = 1039.302\ \text{kJ} \cdot \text{mol}^{-1}$ for both types of bending angle. The torsional angle (ϕ) potential follows the OPLS force field dihedral function, which is defined as [33]:

$$U_{torsional}\left(\phi\right) = \frac{1}{2}k_1\left[1 + \cos\left(\phi\right)\right] + \frac{1}{2}k_2\left[1 - \cos\left(2\phi\right)\right] + \frac{1}{2}k_3\left[1 + \cos\left(3\phi\right)\right] + \frac{1}{2}k_4\left[1 - \cos\left(4\phi\right)\right] \tag{8}$$

The values for the dihedral force constant were obtained from Stubbs et al. [33].

2.3.2. Force Field Parameters for Tetra-PEG Systems

To simulate Tetra-PEG polymer networks consisting of Poly(ethylene oxide) (PEO) chains, we used the modified TraPPE-UA force field [33] with a corrected dihedral potential proposed by Fischer et al. [39] [Eq. (9)], which was found to reproduce well experimental thermodynamics properties of liquid 1,2-dimethoxyethane (DME) in Ref. [39] and the diffusion coefficients and viscosities [40] of $CH_3O(CH_2CH_2O)_nCH_3$ PEO chains in Ref. [38].

Interactions between the three types of united atoms in the chains (i.e., CH_3, CH_2, O) were described by the TraPPE-UA force field [34]; the corresponding LJ parameters are shown in Table S2 in the SI. For Coulombic pairwise interactions, partial charges of 0.25 e, 0.25 e and -0.5 e were used at the centers of the CH_2, CH_3 and O united atoms. The van der Waals and electrostatic interactions were both truncated at 0.9 nm, while long-tail dispersion corrections were treated analytically. The standard Coulombic Ewald method was used to perform the long-range dispersion summation [27]. A harmonic potential [Eq. (6)] was used for the interactions between bonded pairs of united atoms, with equilibrium bond length r_0 of 0.154 nm for $(CH_x - CH_y)_{x,y=2,3}$ and 0.141 nm for $(CH_x - O)$, consistent with the TraPPE-UA force field [34, 38]. The bond stretching constant k_r was 2.92×10^5 kJ $\cdot$ mol^{-1} $\cdot$ nm^{-2} for both types of bonds [23]. Beads separated by two bonds interacted via a harmonic bending potential with energy constants k_θ and equilibrium angle θ_0 of $k_\theta = 1004.239$ kJ $\cdot$ mol^{-1} and $\theta_0 = 112°$ for $CH_x - CH_y - O$ and $k_\theta = 836.436$ kJ $\cdot$ mol^{-1} and $\theta_0 = 112°$ for $CH_x - O - CH_y$.

The torsional potential in the TraPPE-UA force field was modified by Fischer et al. [39] by in order to match the conformer population distribution from ab initio data for 1,2-dimethoxyethane (DME, n=1), the new torsion potential parameters are listed in Table S3 in the SI:

$$U_{torsional}\left(\phi\right)=\sum_{i=0}^{7}k_i\left[1+\cos\left(i\phi\right)\right] \quad (9)$$

The original TraPPE-UA torsional force field does not describe accurately the gauche energy for the COCC dihedral. The modification proposed by Fischer et al. [39] dramatically improves the description of conformer equilibria in both bulk liquid and aqueous solution of DME by the TraPPE-UA force field. For the Tetra-PE network, we also needed to include a torsional potential involving the crosslinking C atom; for this we adopted a TraPPE-UA force field which follows the dihedral function in Eq. (8). The relevant torsional potential parameters are tabulated in Table S4 in the SI.

The pair-wise LJ diameter σ for the carbon atom at the crosslinks was $\sigma(\mathrm{C}) = 0.64\ \mathrm{nm}$ and the energy well depth ε was $\varepsilon(\mathrm{C}) = 0.004157\ \mathrm{kJ \cdot mol^{-1}}$ [41]. There is no partial charge for this type of carbon atom.

We have built two systems (each contains 50 and 150 PEO molecules for n = 5 and n = 9) to validate the implementation of force filed described above for simulating the Tetra-PEG systems. After each system reached equilibrium in an NVT ensemble (T = 303.15 K, with densities set corresponding to 10 bar), the mean square end-to-end distance $\langle r^2 \rangle$ of the PEO chains were calculated by averaging 100 configurations from the last 1 ns. The simulation values agreed well with those from the literature [42] (see Table S5 in the SI).

2.4. Order Parameter and Crystal Fraction

To characterize the crystal fraction of the Tetra-PE diamond network during the crystallization simulations, we adopted the algorithm described by Yi and Rutledge [24] based on a local order

parameter to identify ordered segments in the system. The local $P_2(i)$ order parameter of ith bead is defined as:

$$P_2(i) = \left\langle \frac{3\cos^2\theta_{ij} - 1}{2} \right\rangle_j \tag{10}$$

where θ_{ij} is the angle between the vector from the $(i-1)$th bead to the $(i+1)$th bead, and the vector from the $(j-1)$th bead to the $(j+1)$th bead, and the average is over all the j neighboring beads of bead i that lie within a cutoff distance $r_{ij} < r_{p2}$. The beads with local P_2 near 0 are considered to belong to a disordered amorphous region while beads with P_2 = 1 corresponds to a perfect crystalline state. The global order parameter P_2 was also used to quantify the ordering of the system, which is obtained by the following averaging over all pairs of (i,j) beads in the system regardless of distance:

$$P_2 = \left\langle \frac{3\cos^2\theta_{ij} - 1}{2} \right\rangle_{i \neq j} \tag{11}$$

Besides the cutoff distance r_{p2}, a threshold value $P_{2,th}$ should be chosen so that beads with local P_2 greater than $P_{2,th}$ can be assigned to the crystal phase. The crystal beads i and j are assigned to the same crystal nucleus if the distance between those two beads r_{ij} is less than a threshold value r_{th}. Suitable values for these three parameters, $r_{p2}, P_{2,th}$ and r_{th} have been determined based on simulation results for n-eicosane [24]; for this work we used $r_{p2} = 2.5\sigma, P_{2,th} = 0.4$ and $r_{th} = 1.3\sigma$. We built the n-eicosane system using the TraPPE-UA force field to validate these parameter values and to reproduce the local order $P_2(i)$ probability distribution for a system with one half melted material and the other half crystalline material (see Fig. S2 in the SI), following the method described by Yi and Rutledge [24].

Although the global order parameter of Eq. (11) has been used to determine the melting point of a linear alkane system by Yi and Rutledge [23], it did not capture properly the crystallization behavior for our Tetra-PE network system. Indeed, low values of the global P_2 may not necessary indicate a low crystal fraction in our systems but reflect the presence of multiple crystalline clusters with different alignment (see Figs. S8-S9 in the SI), which may arise due to the constraints associated with the crosslinked structure. Hence we used the local order parameter method to quantify the crystal fraction in the Tetra-PE network, so that all beads with $P_2(i) \geq 0.4$ are considered to belong to the crystal phase.

While the local P_2 order parameter described above is suitable to identify segments in chains that crystalize into zig-zag conformations (as in alkanes), it is unsuitable to monitor the extent of crystallization in chains packing into helical conformation as in the PEO chains [43]. Hence, for Tetra-PEG networks we used a variant of the local P_2 order parameter that has been applied to describe the orientational order of helical polypeptide liquid crystals [44], wherein θ_{ij} in Eq. (10) is defined as angle between the vector from the ith bead to the $(i+d)$ th bead, and the vector from the jth bead to the $(j+d)$ th bead, and the average is over all the j neighboring beads of bead i that lie within a cutoff distance $r_{ij} < r_{p2}$. The choice of "d" determines the "coarse-graining" degree of the helical chains and was found by analyzing a half-melt, half-crystal system of 576 PEO (n=3) molecules using the same approach described above for the n-eicosane system (see Fig. S3 in the SI). The PEO crystal was equilibrated at 276 K and P = 1 atm while the amorphous region was relaxed at T = 500 K and P = 1 atm. As the value d increases, more beads are assigned to the crystal phase ($P_2(i) \geq 0.4$) as shown by the P_2 probability distributions shown in Fig. S4 in the SI. For our ensuing simulations of Tetra-PEG networks, we will use d =

6 as it is the minimal value (least coarse-graining) that correctly identified all the united atoms belonging to the crystalline helical PEO domain.

3. RESULTS AND DISCUSSION

3.1. Tetra-PE Diamond Network Simulations

3.1.1. Crystallization behavior

While Tetra-PE diamond networks with various strand lengths are of interest, for studying the crystallization behavior at temperatures below the melting point, we mainly focus on an n=100 Tetra-PE system as its strands are sufficiently long to form crystal lamellae structure within a reasonable simulation time.

Fig. 1a shows the initial fully extended configuration of the n=100 Tetra-PE diamond network, and Fig. 1b shows the same system upon collapsing into a high-density amorphous network in a 2 ns simulation at T = 303 K, P = 1 atm. After equilibration, the probability distribution of bond lengths, bending angles and torsional angles were calculated by averaging the last 10 simulation snapshots obtained 10000 fs apart. These probability distributions agreed well with the expected Boltzmann distributions (see Figs. S5-S7 in the SI).

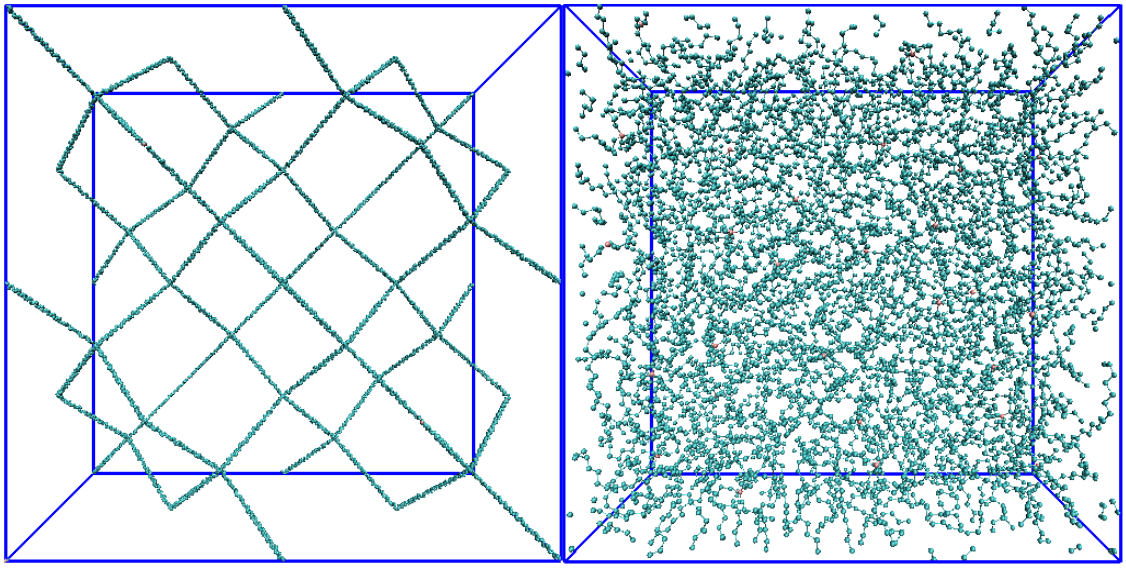

Figure 1 (a) The initial fully extended configuration of the n=100 Tetra-PE diamond network. (b) The same system upon collapsing into a high-density amorphous melt in a 2 ns simulation at T = 303 K, P = 1 atm.

To prepare a representative system containing crystalline material, we performed MD simulations monitoring the nucleation and growth of crystalline domains in the n=100 Tetra-PE diamond network initially in the amorphous state. The crystallization kinetics strongly depends on the degree of supercooling which is the difference between the working temperature T and the melting point T_m. Using as a rough guide the experimental values of $T_m \approx 388$ K [45] and $T_g \approx$ 143 K [46] for the glass transition temperature of for linear polyethylene, we chose a supercooled state with temperature T = 260 K for our crystallization simulations (initially prepared by gradually cooling a pre-equilibrated sample at 303 K). Fig. 2 shows the increase in crystal fraction as the system was equilibrated at 260 K and P = 1 atm. After the crystal nucleus emerges [see Fig. 3 (left)], the crystal fraction grows approximately linearly with time, up to about 60 ns when the growth of lamellae begins to slow down. During crystal growth, the network strands begin to align with the neighboring polymer chains, aggregating into several crystal clusters [see Fig. 3 (right)]. The size of the crystal clusters continued to increase and merge into larger

lamellae. The simulation was stopped when the crystal fraction had reached a plateau, in our case corresponding to about 40% crystallinity, as subsequent crystal growth is very slow and would require a very large investment of computing resources. Note, however, that one would not expect complete crystallization given the topology of the network and the presence of crosslinks, which tend to be excluded from ordered domains. Snapshots of the resulting semicrystalline network with unwrapped coordinate at 120 ns are shown in Fig. 4a; the hexagonal packing of the polyethylene chains formed within a lamellar structure [47] is evident from the side view in Fig. 4b.

Since the kinetics of crystallization of the network depend on the state of strain of the sample, we also repeated the simulation starting with an amorphous system at a strain of $\varepsilon = 1$ (keeping constant the length of the box along the deformation direction) at T = 260 K and P = 1 atm. The results (also shown in Fig. 2) exhibit a faster crystal growth during the first 80 ns (e.g., to attain 15% crystallinity it now only took 25 ns while it took 60 ns in the unstrained sample), followed by a slow growth thereafter. However, the total crystal fraction at the end of 200 ns (namely ~ 40%) is essentially the same in both cases.

Finally, we note that Tetra-PE networks with n<100 are more difficult to (partially) crystallize. For example, simulations at 260 K and 1 atm show that an n=30 Tetra-PE network produced less than 1% of crystalline material after 190 ns while an n=18 Tetra-PE network formed no detectable crystalline trace after 220 ns. This is partially due to the local disordering effect that crosslinks have (akin to branching points in PE), and since shorter n networks have a higher concentration of crosslinks, they also experience a larger hindrance to crystallization. Besides such structural effects, a segmental dynamic slowing down is also detectable in networks with shorter strands. This can be quantified by the short time behavior of the mean-squared-

displacement (MSD) of the middle atoms of the network strands (MSDm) and of the crosslinks (MSDx) of the Tetra-PE networks of various strand lengths (Fig. 5) at T = 260 K and P = 1 atm. Clearly, the segmental mobility (as measured, e.g., by the MSD for a fixed simulation time) - needed to cooperatively align multiple strands - decreases rapidly with smaller n.

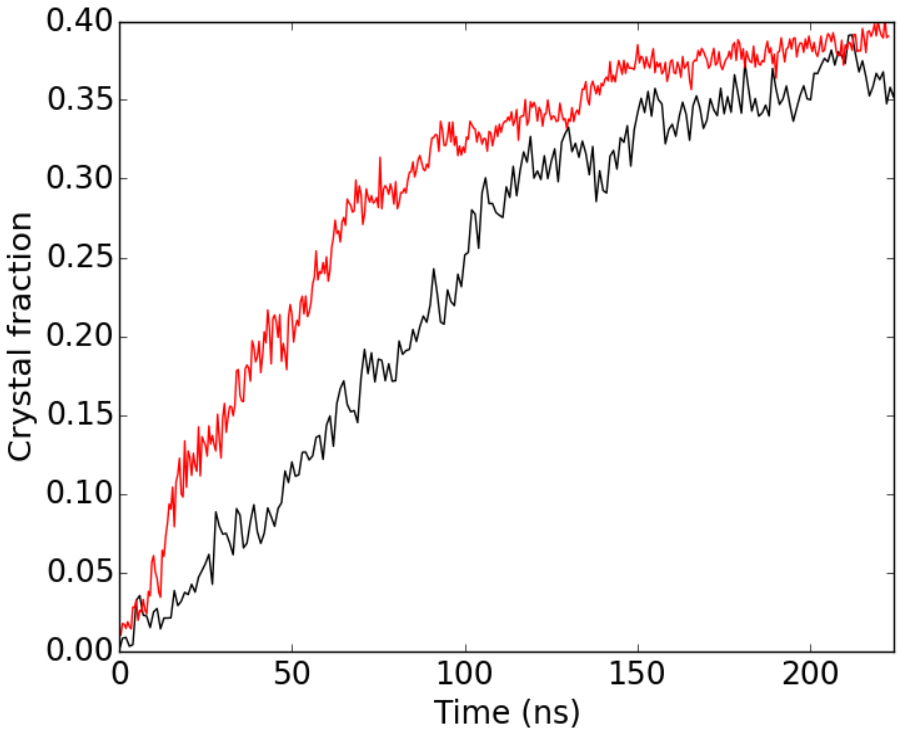

Figure 1 Evolution of the crystal fraction with time in the n=100 Tetra-PE diamond network at T = 260 K and P = 1 atm (black: the undeformed sample; red: the pre-deformed amorphous system kept at $\varepsilon = 1$).

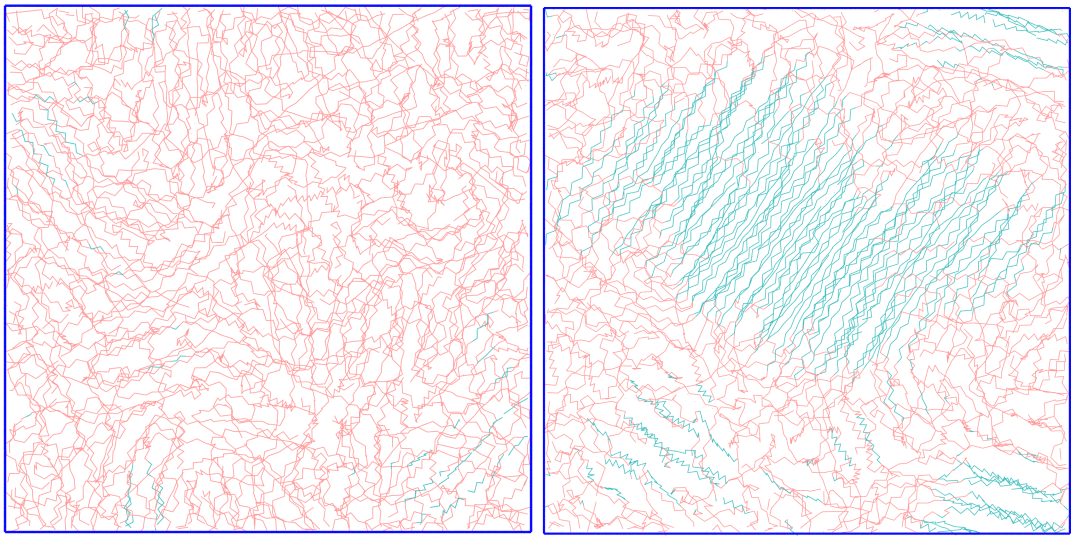

Figure 2 Spontaneous crystallization in the n=100 Tetra-PE diamond network at T = 260 K and P = 1 atm. Left Emergence of aligned bundles after 1 ns of equilibration. Right: Crystal clusters forming a larger lamellae after 250 ns of equilibration when the system reached about 40% crystallinity. Red/cyan denote amorphous/crystalline segments. All atoms have been wrapped into the simulation box.

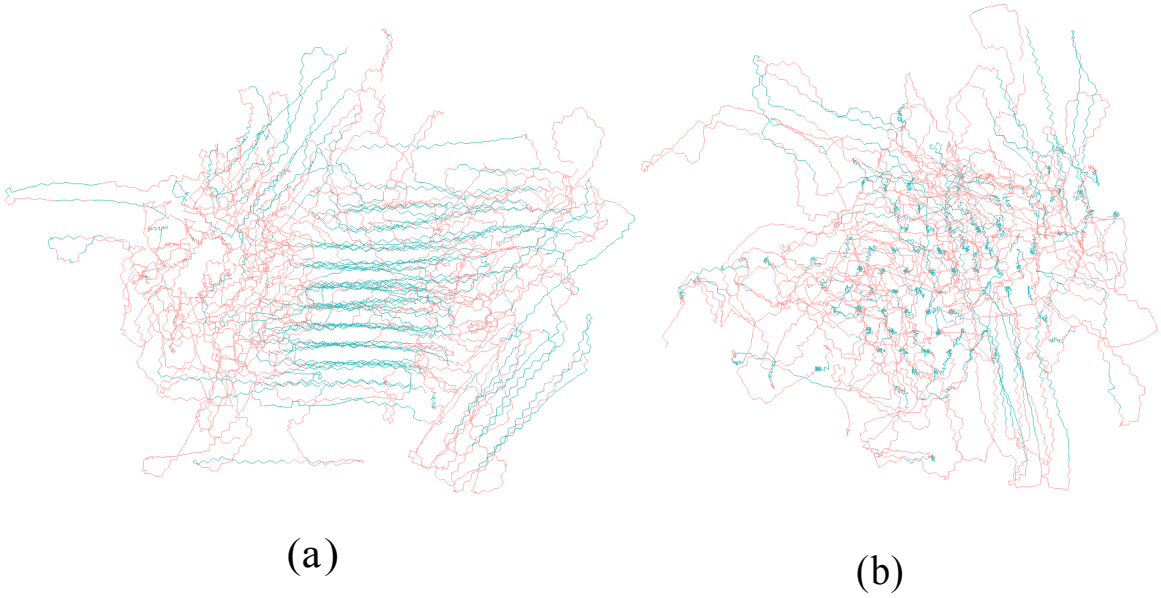

Figure 3 Two orthogonal perspectives of the lamellar structure formed in the n=100 Tetra-PE diamond network at 260 K (40% crystallinity), with chains shown in unwrapped representation. (a) The polyethylene chains aggregate to form locally folded domains. (b) The side view of the system showing the expected hexagonal packing of chains.

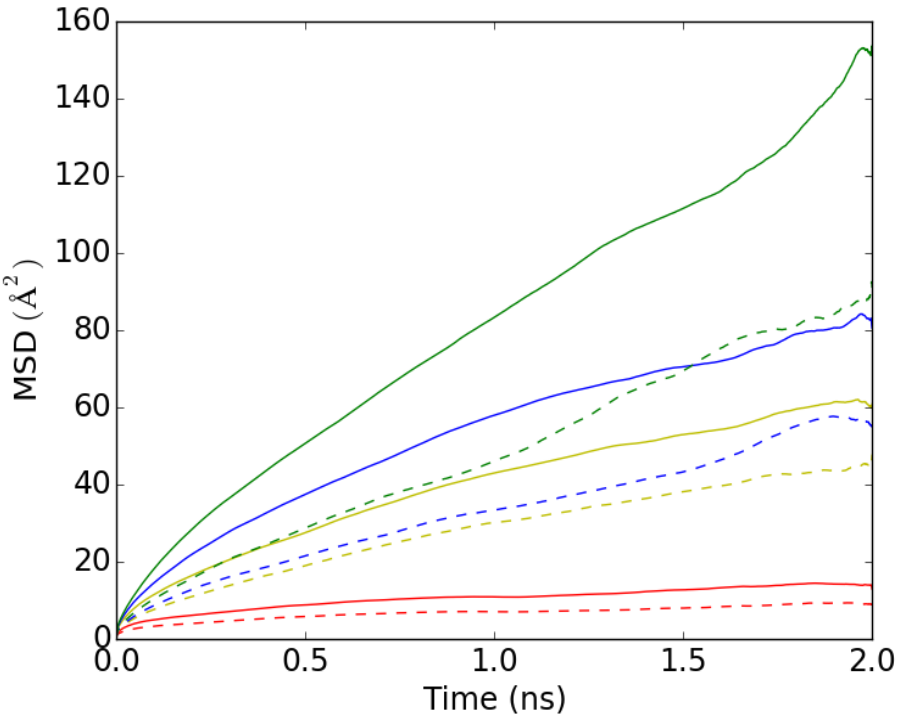

Figure 5 Mean-squared-displacement of the middle atoms of the network strands (solid line) and of the crosslinks (dashed line) of amorphous Tetra-PE diamond networks equilibrated at T = 260 K, P = 1 atm, with degree of polymerization n = 6 (red), 18 (yellow), 30 (blue), and 100 (green). All samples were in the amorphous state during the simulations. The complete data are shown in Fig. S10 in the SI.

3.1.2. Melting Point Estimation in the n=100 Tetra-PE

The equilibrium melting point T_m is a key reference in analyzing the crystallization behavior of the Tetra-PE network system. By monitoring the changes in the degree of crystallinity of a network with an initial 40% crystallinity (as described before), we estimated T_m by using MD isothermal-isobaric simulations to equilibrate the system at different temperatures (and P = 1 atm). The simulations were 310 ns long and the equilibrium density and crystal fraction were obtained by averaging the last 10 snapshots collected 10000 fs apart. The normalized density and the crystal fraction of the system at different temperatures are plotted in Fig. 6 (the evolution of crystal fraction over the last 20 ns of simulation is shown in Fig. S9 in the SI). The abrupt change in density and crystal fraction in Fig. 6 signals the presence of a phase transition from a stable

semicrystalline state to a fully amorphous state. Based on these results, the melting point T_m was estimated to be between 315 K and 320 K.

Luo et al. [48] suggested that the melting temperature of polyethylene would decrease with increasing of degrees of branching (DB). The simulated equilibrium density of the n=100 Tetra-PE system is 0.875 $g \cdot cm^{-3}$ at T = 280 K, P = 1 atm. For polyethylene with density of 0.850 $g \cdot cm^{-3}$ at 273 K and 1 atm, molecular weight of 110.1 $kg \cdot mol^{-1}$ and DB = 0.258, the experimental T_m is 319.3 K [48], a value that suggests that the estimated T_m for our network is reasonable. It is worth noting that the TraPPE-UA force field was originally developed to reproduce vapor-liquid coexistence properties of fluids [49] (not solid-liquid coexistence properties) and hence one should not expect T_m estimates to be very accurate.

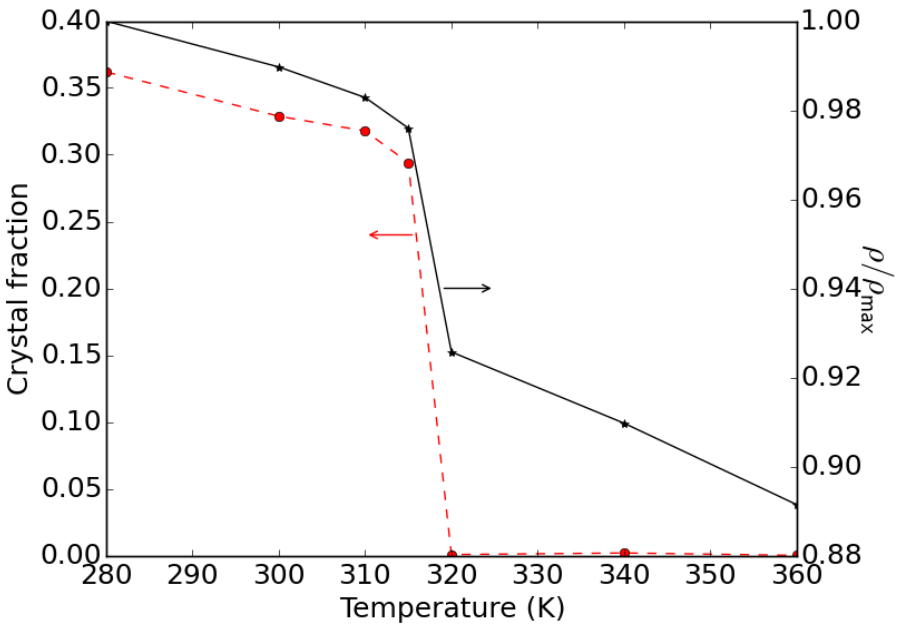

Figure 6 The normalized density and crystal fraction of the n=100 Tetra-PE diamond network equilibrated at different temperatures.

3.1.3. Influence of Crystal Content on Stress-Strain Relation

To study the effect of crystal content on the stress-strain relation, we performed uniaxial deformation simulations on two n=100 Tetra-PE systems having different initial crystal fraction in the undeformed state: (1) A purely amorphous sample pre-equilibrated at 360 K and 1 atm, and (2) the semi-crystalline system with 40% crystal fraction obtained at 260 K (as described above). The uniaxial deformation was performed using an NVT ensemble at T = 260 K and strain rate $\dot{r} = 2.5 \times 10^{-6}$ fs^{-1}. This comparison is in line with the assumption that it is experimentally possible to process polymer samples to attain different extents of crystal content at a temperature below the melting point.

Our results shown in Fig. 7 indicate that the sample with higher initial crystalline fraction exhibits a higher stress at the same strain during deformation. This is consistent with typical trends observed experimentally [50]; e.g., the tension in an elongated rubber that has undergone crystallization during stretching has been found to be substantially greater than in a similar rubber in which no crystallization occurs at the same elongation [51]. This is because the presence of crystal domains increases the coupling among the conformations of the multiple strands connected to them, causing an additional resistance to deformation. Note that both samples gradually increase the amount of crystalline material during elongation, a process whose kinetics likely depends on strain rate.

A distinct feature of the stress-strain curves in Fig. 7 is a drastic increase in the tensile response at high strain values (near ε = 13), where all chains in the network become highly stretched, while the crystal fraction approaches unity. Since all of our simulations use harmonic potential for bonding interactions without a bond breakage mechanism, the stress would keep increasing as the bonds continue to be stretched further.

We have observed that the deformation process exhibits large hysteresis; that is, when the system is allowed to relax (by removing any strain constraint), the deformed polymer network does not recoil back to its unstrained state. For instance, a sample of n=100 Tetra-PE deformed to $\varepsilon = 6$ that was relaxed under constant pressure (P = 1 atm) conditions along all axes at T = 303 K only recoiled by 3.5% after 20 ns. This is likely a consequence of the irreversible nature of the strain-induced crystallization which tend to "freeze" a particular structure for the chains; this observation is also consistent with simulation results of Aguilera et al. [8] where pronounced hysteresis was also observed between loading and unloading runs of coarse-grained diamond networks that formed multiple smectic domains upon straining.

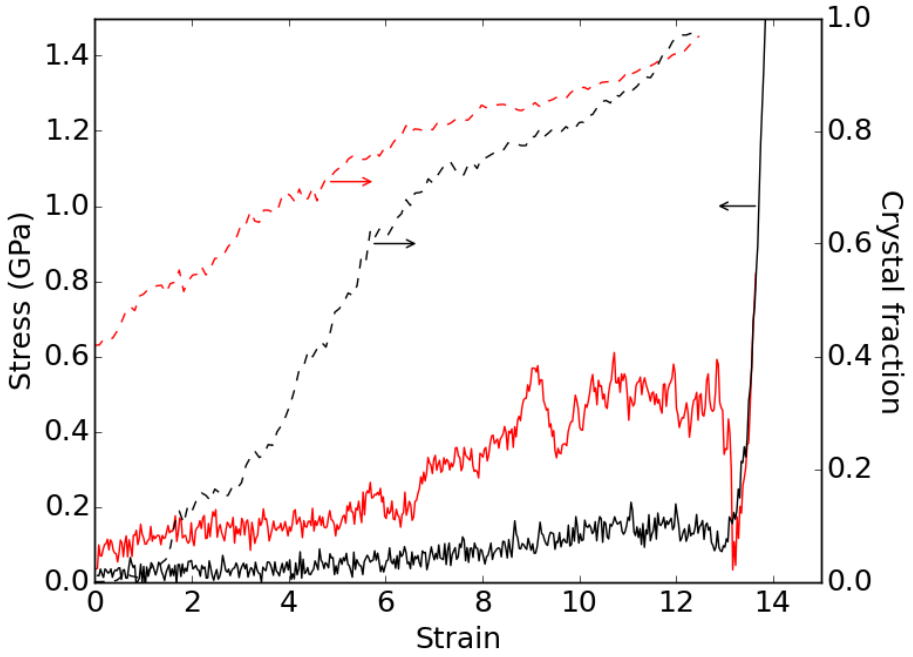

Figure 7 Stress-strain and crystal fraction vs. strain from uniaxial deformation simulations of the n=100 Tetra-PE diamond network using an NVT ensemble at T = 260 K and strain rate $\dot{r} = 2.5\times10^{-6}$ fs^{-1}. Color identifies undeformed state: Black = amorphous sample; red = semi-crystalline system with 40% crystal content.

3.1.4. Influence of Chain Length on the Stress-Strain Relation

To understand the effect of chain length on the stress-strain relation, we performed uniaxial deformation simulations for 7 different Tetra-PE diamond networks of various strand lengths n

in the strain-driven (NVT) ensemble at T = 303 K. Since the melting point temperature typically increases with polymer molecular weight for short chain system [52], the melting point temperature of Tetra-PE systems with n<100 would be expected to be lower than that of n=100 Tetra-PE system. This trend is only a rough guide since its application is questionable to polymer networks whose molecular weight can be seen as being essentially "infinite" (regardless of n). With such a caveat notwithstanding, we surmise that at 303 K all systems are likely either above their T_m or so mildly undercooled that the amorphous states is metastable (and hence it is experimentally viable to process them into amorphous samples). Accordingly, the systems prepared for our simulations were in a fully amorphous state, i.e., the crystalline fraction is zero at the undeformed state.

The uniaxial deformation simulations were carried out at a constant engineering strain rate of $\dot{r} = 2.5 \times 10^{-6}$ fs^{-1} until the network strands were fully stretched and aligned with the deformation axis. We performed uniaxial deformation simulations for the n=100 Tetra-PE systems at a strain rate ten times higher and found that it has some influence in the stress response; i.e., the higher strain rate gives higher stress values as well as lower crystal fraction (for a given strain) than those for the lower strain rate, an effect that is coupled to the concurrent strain-driven crystallization process (see Fig. S11 in the SI). While the stain rate $\dot{r} = 2.5 \times 10^{-6}$ fs^{-1} is still very large compared to typical experiments, it is near the lower end of values that have been employed in similar simulation studies. Fig. 8 shows the stress-strain curves for Tetra-PE networks of various strand lengths. The initial linear regions of the stress-strain curves of the systems tend to overlap, suggesting that the Young's modulus of the diamond networks, measured as the ratio of stress to strain at small strains, is weakly dependent on the degree of polymerization of the network

strands (see Table S6 in the SI). The value of n affects primarily the maximum elastic extensibility of the diamond network.

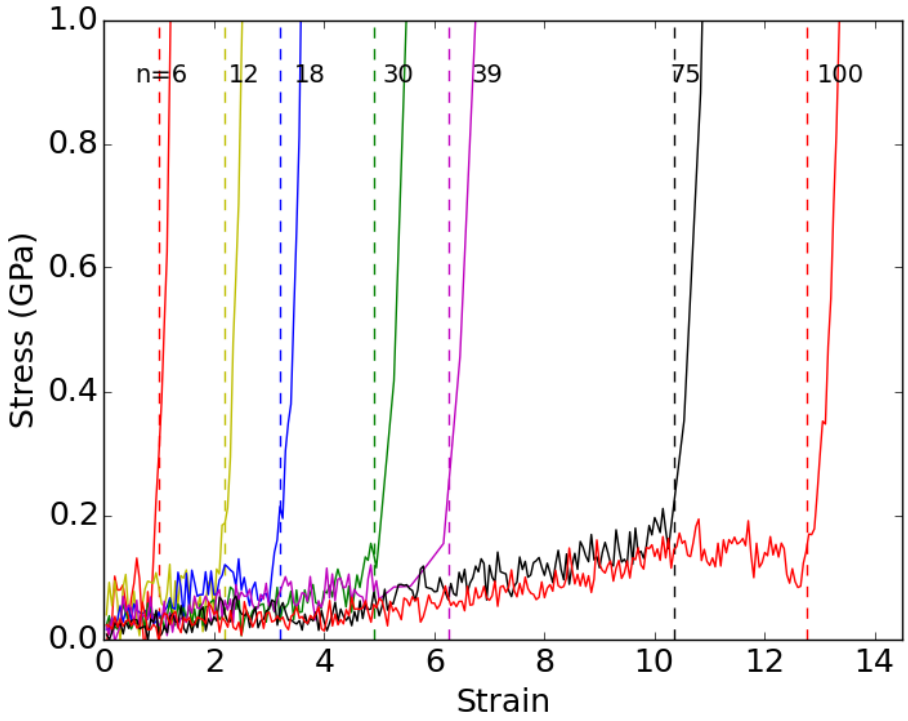

Figure 8 The dependence of stress-strain behavior on degree of polyermization of the Tetra-PE diamond network strands at T = 303 K. The predictions of Eq. (12) for the strain ε^* where the upturn in stress occurs are plotted as vertical dash lines.

Despite the noise in the stress data at low strains, it is possible roughly estimate the Young's modulus in the linear regime for $75 \leq n \leq 100$: $E \sim 0.01$ GPa (see Fig. S12 in the SI), a value that is comparable to silicone elastomer ($E \sim 0.011$ GPa) [53] and Ethylene vinyl Acetate (EVA) copolymers ($E \sim 0.012$ GPa) [54]. The stress-strain curves show that as the strand length increases, the Young's modulus decreases slightly, indicating that the network becomes more elastic and softer.

Since the diamond network is homogenous and free of trapped entanglement, the chains can unravel and align completely without trapping entanglements upon stretching. Our amorphous

polymer diamond networks hence exhibit a small stress response (i.e., soft response) over a wide range of strains where network chains are allowed to stretch while freely inter-dispersing.

For large deformations where chains become highly aligned with the deformation axis, the crosslinks of the diamond network distribute evenly into different segregated groups. For example, Fig. 9 shows the n=12 Tetra-PE diamond network at strains of 2.0 and 2.5, where the crosslinks segregate into eight distinct domains. This segregation phenomenon begins to happen before the stress upturn sets in, and it has been observed for all strand lengths simulated. Segregation of crosslinks and smectic chain domains was also observed by Aguilera et al. [8] upon uniaxial deformation of a diamond network with coarse-grained semiflexible chains, where the number of such domains increased with strain through discrete events, each eliciting a spike in stress and hence producing a "saw-tooth" stress response. It is unclear why such a saw-tooth behavior is absent in our systems, but it could be a reflection of the importance of molecular details in shaping microstructure and in how strain-induced structural rearrangements couple with stress.

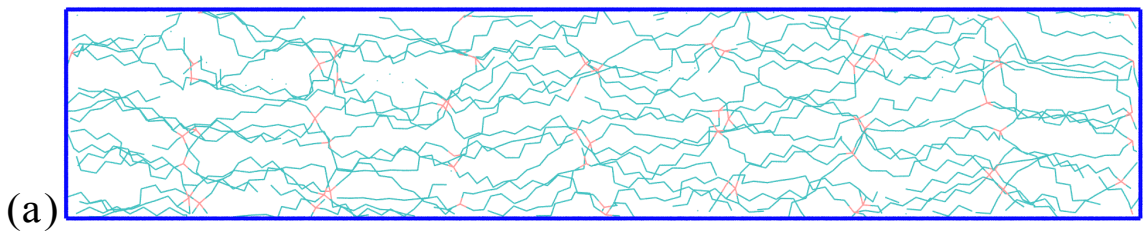

(a)

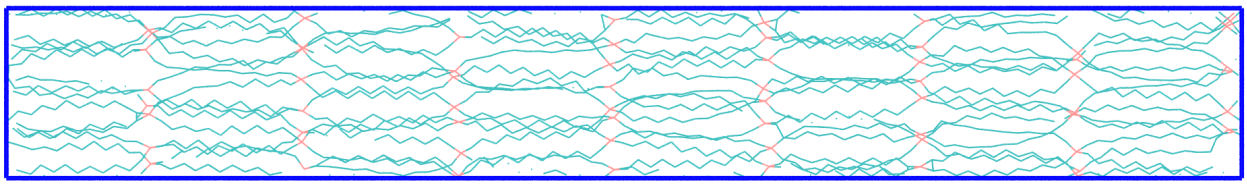

(b)

Figure 9 Snapshot of an n=12 Tetra-PE diamond network deformed at the strain of: (a) ε = 2.0 and (b) ε = 2.5. The crosslinks (shown in red) segregate into eight separate domains.

The rapid upturn in stress signals the point where all network strands are almost completely stretched. Since there is no bond breaking mechanism introduced in our systems, the stress keeps increasing as all bonds are stretched further. In reality, bond breakage will start occurring some time after the stress upturn appears. Note, however, that the absence of topological defects in these networks implies that at high elongations no weak links will initiate breakage events and hence all chemical bonds will be concurrently engaged, potentially leading to very high ultimate stresses. The tensile strength, which is defined as the maximum tensile stress a sample can take before failure, is conservatively estimated for our systems at the point right before the stress upturn occurs. For the n=100 Tetra-PE diamond network this corresponds to ~200 MPa, which is significantly higher than that of low density polyethylene (LDPE) (ρ = 0.925 $\mathrm{g \cdot cm^{-3}}$) which is 9.1 MPa [55].

The strain ε^* where the upturn in stress occurs is a metric of the polymer extensibility and can be related to the strand length as follows. Assuming that all Tetra-PE systems have the same equilibrium density ρ at 0.875 $\mathrm{g \cdot cm^{-3}}$ and that the length of the box L^* along the deformation axis at the strain ε^* is equal to the total length of 8 groups of fully stretched strands, then:

$$\varepsilon^* = \frac{L^*}{L_0} - 1 = \frac{8 \cdot n \cdot l_b}{\left(\frac{m}{\rho}\right)^{\frac{1}{3}}} - 1 = \frac{8 \cdot n \cdot l_b}{\left(\frac{128 \cdot n \cdot M_{CH_2}}{N_A \cdot \rho}\right)^{\frac{1}{3}}} - 1 = k \cdot n^{\frac{2}{3}} - 1 \qquad (12)$$

where the bond length l_b is assumed to be 1.2 Å by taking account the zig-zag conformation of the chain backbones and the projections of the bonds along the z axis; M_{CH_2} = 14 $\mathrm{g \cdot mol^{-1}}$, N_A is Avogadro constant; hence the coefficient k is ~ 0.635. Equation (12) is in line with the empirical

expression often used to determine the experimental elongation ratio at break λ_{break} for networks which can be expressed as [18]: $\lambda_{break} \sim N_c^{0.71}$ where N_c is degree of polymerization, noting that elongation λ and strain ε are related by:

$$\varepsilon = \frac{L}{L_0} - 1 = \lambda - 1$$

The predictions of strain ε^* where the stress upturn occurs based on Eq. (12) agree well with simulation results (see dashed lines in Fig. 8).

3.2. Tetra-PEG Diamond Network Simulations

A total of 7 Tetra-PEG diamond network systems were built with degree of polymerization [or number of $(-CH_2CH_2O-)$ groups on each network strand] n = 1, 3, 5, 9, 12, 24 and 40. The initial fully extended configuration of an n=5 Tetra-PEG diamond network and the configuration upon collapsing into an amorphous melt in a 2 ns simulation at T = 303 K, P = 1 atm are shown in Fig. S13 in the SI.

The equilibrium density and box dimension of Tetra-PEG diamond networks after 2 ns simulation at T = 303 K and P = 1 atm are shown in Table 1. The equilibrium density of the n=40 Tetra-PEG system is close to the experimental density (ρ = 1.17 $g \cdot cm^{-3}$) of a dried Tetra-PEG amorphous material with molecular weight of its pre-polymers M_{pre} = 10 $kg \cdot mol^{-1}$ corresponding to degree of polymerization n=110 on each network strand [4].

Table 1 Simulation results of Tetra-PEG diamond networks (n = 1 to 40) at T = 303 K and P = 1 atm; N indicates the number of united atoms in each system. The equilibrium density is the average of 100 configurations from the last 1 ns after the density reached a plateau.

n	N	Equilibrium Density (g/cm^3)	Box Dimension
1	832	1.053 ± 0.042	$L_x = L_y = L_z$ (Cubic Box)
3	1600	1.119 ± 0.024	
5	2368	1.153 ± 0.019	
9	3904	1.156 ± 0.016	
12	5056	1.157 ± 0.014	
24	4832	1.166 ± 0.015	$L_x = L_y = 2 \times L_z$ (Half Cubic Box)
40	7904	1.166 ± 0.011	

3.2.1. Mean-Squared-Displacement of the Middle Atoms of Strands and the Crosslinks

To estimate the melting point T_m of Tetra-PEG diamond networks, we attempted crystallization simulations of amorphous Tetra-PEG diamond networks at a supercooled temperature of T = 260 K at P = 1 atm (for reference, the experimental T_m for PEO with n=68 range between 332.2 K to 333.5 K, with $T_g \approx 213$ K [56]). However, 220 ns long simulations failed to seed any detectable amount of crystalline material. This failure correlates with our observation of simulation trajectories that show that the motions of the network beads in these systems are significantly slower than those of the Tetra-PE systems at the same conditions. To quantify this difference, we simulated the mean-squared-displacement of the middle atoms of the network strands (MSDm) and of the crosslinks (MSDx) of Tetra-PEG networks at T = 260 K and P = 1 atm (Fig. 10) and compared them to those for the Tetra-PE networks shown in Fig. 5. In general, the values for either MSDm or MSDx at any given time are over an order of magnitude larger for the Tetra-PE systems than for the Tetra-PEG systems (see also comparison in Fig. S15 in the SI). Physically, this difference seems to be rooted in the stronger Coulombic intermolecular interactions that physically associate the PEO segments (interactions absent in the PE strands). For all strand lengths we simulated for the Tetra-PEG networks, the motions of the network beads are significantly limited, which hinders chain folding and realignment, thereby inhibiting the

crystallization process (not unlike the situation we described before for short-stranded Tetra-PE networks). Although we could attempt to simulate Tetra-PEG systems with much longer n, the larger system sizes associated with it would create additional challenges (note that the effective strand length –in terms of number of united atoms - of an n=40 Tetra-PEG networks is comparable to that of an n=123 Tetra-PE network). We hence forsake the estimation of a melting transition for Tetra-PEG networks given that spontaneous crystallization simulations at large supercooling would involve a prohibitive investment of our current computing resources. As an imperfect surrogate, we did estimate the melting temperature T_m of PEO chains with n=30 to be between 350 K to 360 K (as described in Figs. S16-S17 of the SI), which suggest that networks at room temperature could contain semicrystalline material.

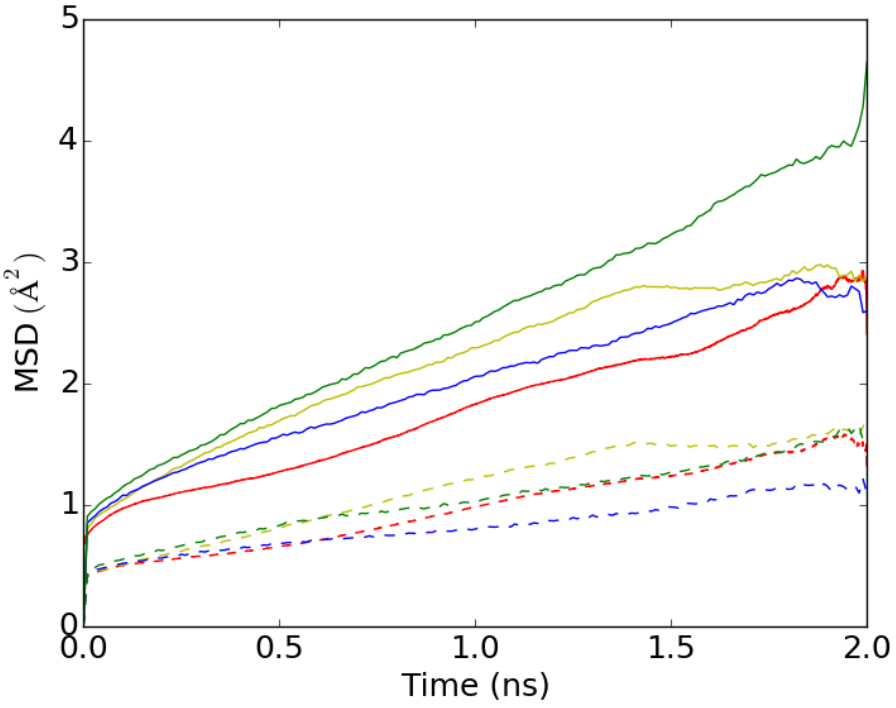

Figure 10 Mean-squared-displacement of the middle atoms of the network strands (solid line) and of the crosslinks (dash line) of amorphous Tetra-PEG systems equilibrated at T = 260 K, P = 1 atm, with degree of polymerization n = 3 (red), 9 (blue), 12 (yellow), and 40 (green). The complete data are shown in Fig. S14 in the SI.

3.2.2. Uniaxial Stress-Driven Deformation

Based on the simulation protocol described in Section 2.2 for simulating Tetra-PE diamond networks, we performed uniaxial deformation simulations for 7 different amorphous Tetra-PEG diamond networks to investigate the effect of the chain length on the stress-strain relation. Fig. 11 shows the stress-strain curves obtained for a strain rate of $\dot{r} = 2.5 \times 10^{-6}$ fs^{-1} at 303 K. The predictions for the strain ε^* where the upturn in stress occurs suggests that the Tetra-PEG networks have an extensibility similiar to the Tetra-PE networks having same strand molecular weight (see also Fig. 11). Similar to Tetra-PE networks, the initial partial overlap in the stress-strain cuves of the Tetra-PEG networks shows that at low strain, the Young's modulus is weakly dependent on the length of the network strands (see also Table S7 in the SI).

However, the Young's moduli of Tetra-PEG diamond networks are nearly 10 times larger than those of Tetra-PE systems having similar strand molecular weight, which suggests that Tetra-PEG diamond networks are significantly stiffer than their Tetra-PE conterparts at the amorphous state. The Young's modulus of an n=40 Tetra-PEG diamond network ($E \sim 0.14$ GPa) (see Fig. S18 in the SI) is comparable to that of the ionomer Nafion ($E \sim 0.1$ GPa) [57]. Katashima et al. [18] reported that the Young's modulus for a completely dried amorphous Tetra-PEG (M_{pre} = 10 K, n ≈ 110) obtained at 55 ^{o}C was about 4 MPa, which is significantly smaller than 140 MPa for our n=40 Tetra-PEG network. The stress-strain curves for Tetra-PEG systems of various strand lengths show that systems with longer chain length have lower elastic Young's modulus, hence the Young's modulus of the n=40 Tetra-PEG network is expected to be much larger than that of the experimental amorphous, dried sample of Tetra-PEG having n=110. Moreover, as the amount of defects in a network increases, the stress response to strain decreases [19]; since a well

synthesized Tetra-PEG material typically has at least 5% of topological defects [13], one would expect a higher Young's modulus from our defect-free Tetra-PEG diamond network.

Our Tetra-PEG diamond networks have estimated tensile strengths (the maximum stress a network can take "before" the stress upturn occurs in the stress-strain curve) between 4 and 6 GPa, which is much larger than the 0.2 GPa of Tetra-PE diamond networks. The tensile strength of Tetra-PEG diamond network would also be larger than previously reported values for composite fibers of single-walled nano-tubes (SWNTs, with tensile strength of 1.8 GPa [58]), and for spider silk with 1.1 GPa [59].

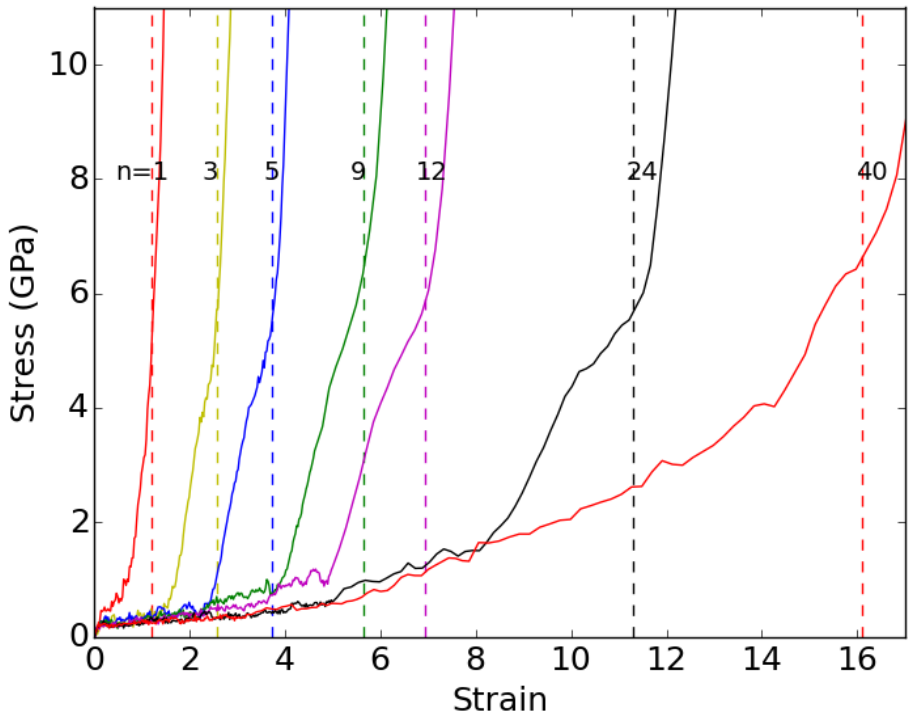

Figure 11 The dependence of stress-strain behavior on degree of polyermization of the Tetra-PEG diamond networks. The predictions of Eq. (12) for strain ε^* where the upturn in stress occurs are plotted as vertical dash lines.

An interesting feature in Fig. 11 is the "stress hump" that appears in the stress-strain curve between the linear region and the stress upturn. To understand the origin of this feature, we monitored the change in crystal fraction during deformation for the n=24 Tetra-PEG diamond

network at 303 K, using the modified local order parameter described in Section 2.3.3, as shown in Fig. 12. The point when the value of crystal fraction reaches unity indicates that all the helical PEO chains have aligned with the deformation axis and have fully crystallized. Further deformation causes a transition of the network strands from helical into zig-zag conformation [43, 60] (see also Fig. 13). The "stress hump" in the stress-strain curve is hence due to the resistance associated with the deformation of helical PEO chains which act like "springs". Note that these "stress humps" would tend to be smeared out for longer chain lengths and for larger systems sizes. Finally, we note that at the high strains where these humps happen, the crosslinks segregate into 8 groups in a manner similar to that seen before for the Tetra-PE networks (in Fig. 13 the crosslink groups do not appear as only a small portion of the sample is shown for clarity).

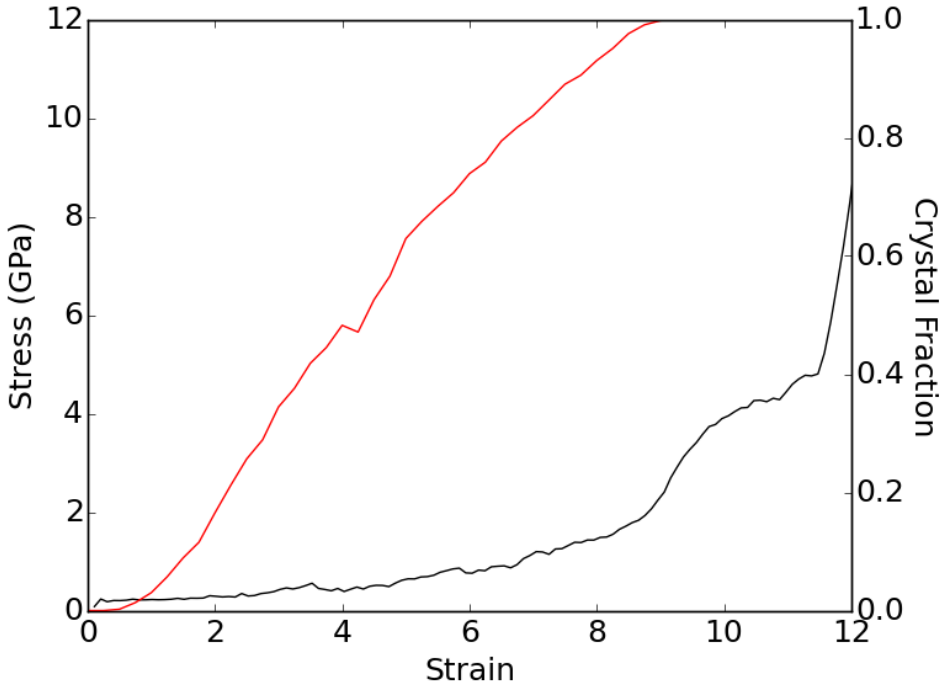

Figure 12 Stress-strain curve (black) and crystal fraction (red) during the elongation of an n=24 Tetra-PEG diamond network at T = 303 K.

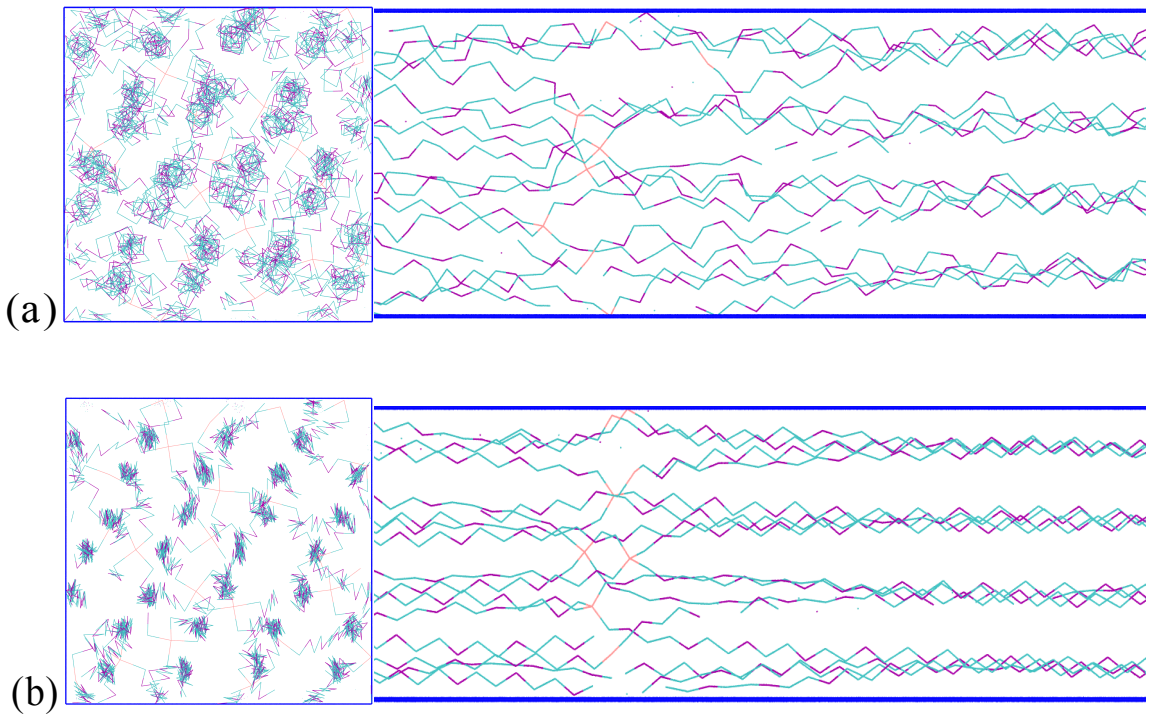

Figure 13 Network strands of the n=24 Tetra-PEG diamond network: (a) at strain ε = 9.3 showing helical conformations and (b) at strain ε = 12 showing zig-zag conformations. In both cases the left panel shows a view into the deformation axis and the right panel shows a partial side view along the deformation axis.

4. CONCLUSIONS

In this study, we investigated the mechanical properties of Tetra-PE and Tetra-PEG diamond networks of various strand lengths using atomistic molecular dynamics simulations based on realistic force field potentials. Since such properties are affected by the presence of or proclivity to form crystalline material in the undeformed samples, we examine first whether (semi) crystalline networks could be prepared and their melting behavior characterized. To estimate the melting point of the Tetra-PE diamond networks, we prepared a semi-crystalline sample of an n=100 Tetra-PE diamond network and identified the temperature at which the crystal fraction in the system changed abruptly (signaling a phase transition from a stable semi-crystalline state to a

fully amorphous state). The melting point T_m thus obtained was consistent with experimental T_m values for branched polyethylene-based materials.

Through the exploration of the effect of crystal content on the stress-strain relation of the Tetra-PE networks, we found that the sample with higher crystal fraction exhibits higher stress at the same strain during deformation, a result consistent with experimental observations with elongated rubbers undergoing crystallization during stretching.

Examination of the mean-squared-displacement of the middle atoms of the network strands and of the crosslinks of Tetra-PE and Tetra-PEG diamond networks showed that short strand lengths hinder chain folding and inhibit the crystallization process in unstrained amorphous samples. It also revealed that the chain motions of Tetra-PEG diamond networks, necessary for spontaneous chain ordering, are significantly slower than those of Tetra-PE diamond networks having similar strand molecular weight. Crystallization simulations of Tetra-PEG networks at supercooled conditions were unsuccessful for the system sizes and simulation lengths that were practicable with available computational resources.

Simulations of the stress-strain relation obtained from uniaxial deformation of Tetra-PE and Tetra-PEG networks of various strand lengths revealed that the Young's modulus weakly depend on the length of the network strands at low strain for both chemistries. Tetra-PE and Tetra-PEG diamond networks with the same strand length have comparable maximum extensibility but the Young's moduli of the former are significantly lower than those of the latter, a reflection of stronger intersegmental interactions in the amorphous Tetra-PEG networks. The high tensile strength that such defect-free diamond networks could attain, suggests that these materials would exhibit super-toughness qualities that hold great appeal in a broad range of applications.

Our highly idealized model provides a starting point for the systematic study of near-perfect diamond networks to assess the effect of topological defects, chain length polydispersity, trapped entanglements, and different monomer chemistries. Future studies could therefore consider realistically generated network samples by using molecular simulations to mimic the crosslinking process [61-63]. Ultimately, this and follow-up studies will provide guidance to the design and analysis of novel polymer networks with desirable *super* tensile properties.

Since most of the reported experimental results of Tetra-PEG have been obtained for samples swollen in water (i.e., gels), we are unable to use them for comparisons with our results (which are restricted to completely dried systems). It would be of interest to develop simulation models that would allow studying the swelling behavior and mechanical properties of Tetra-PEG gels; e.g., by using suitable parameterized force fields that account for solvation of chains in (implicit) water. Research along these lines is under way.

Acknowledgements

This work was supported by the National Science Foundation award CMMI 1435852.

Reference:

1. Escobedo, F.A. and J.J. de Pablo, *Monte Carlo simulation of branched and crosslinked polymers.* The Journal of chemical physics, 1996. **104**(12): p. 4788-4801.
2. Chen, G., et al., *Tissue engineering of cartilage using a hybrid scaffold of synthetic polymer and collagen.* Tissue Engineering, 2004. **10**(3-4): p. 323-330.
3. Escobedo, F.A. and J.J. de Pablo, *Phase behaviour of model polymeric networks and gels.* Molecular Physics, 1997. **90**(3): p. 437-444.
4. Nomoto, Y., et al., *Structure and physical properties of dried Tetra-PEG gel.* Polymer, 2011. **52**(18): p. 4123-4128.
5. Everaers, R. and K. Kremer, *Test of the foundations of classical rubber elasticity.* Macromolecules, 1995. **28**(21): p. 7291-7294.
6. Everaers, R., *Entanglement effects in defect-free model polymer networks.* New Journal of Physics, 1999. **1**(1): p. 12.
7. Everaers, R. and K. Kremer, *Test of the Foundations of Classical Rubber Elasticity.* Macromolecules, 1995. **28**: p. 7291.
8. Aguilera-Mercado, B.M., C. Cohen, and F.A. Escobedo, *Sawtooth Tensile Response of Model Semiflexible and Block Copolymer Elastomers.* Macromolecules, 2014. **47**(2): p. 840-850.
9. Bhawe, D.M., C. Cohen, and F.A. Escobedo, *Stepwise elastic behavior in a model elastomer.* Physical review letters, 2004. **93**(25): p. 257804.
10. Schneider, S. and P. Linse, *Monte Carlo simulation of defect-free cross-linked polyelectrolyte gels.* The Journal of Physical Chemistry B, 2003. **107**(32): p. 8030-8040.
11. Bhawe, D.M., C. Cohen, and F.A. Escobedo, *Formation and characterization of semiflexible polymer networks via monte carlo simulations.* Macromolecules, 2004. **37**(10): p. 3924-3933.
12. Sakai, T., et al., *Design and fabrication of a high-strength hydrogel with ideally homogeneous network structure from tetrahedron-like macromonomers.* Macromolecules, 2008. **41**(14): p. 5379-5384.
13. Akagi, Y., et al., *Evaluation of topological defects in tetra-PEG gels.* Macromolecules, 2009. **43**(1): p. 488-493.
14. Sugimura, A., et al., *Mechanical properties of a polymer network of Tetra-PEG gel.* Polymer journal, 2012. **45**(3): p. 300-306.

15. Takehara, H., et al. *Hydrogel reactive microbonding (HRMB) method for the use of tetra-PEG gel as a structural material for microfluidic devices*. in *Proc. Micro Total Analysis Systems*. 2011.
16. Li, X., et al., *Precise control and prediction of hydrogel degradation behavior.* Macromolecules, 2011. **44**(9): p. 3567-3571.
17. Nishi, K., et al., *Kinetic Aspect on Gelation Mechanism of Tetra-PEG Hydrogel.* Macromolecules, 2014. **47**(10): p. 3274-3281.
18. Katashima, T., et al., *Mechanical properties of tetra-PEG gels with supercoiled network structure.* The Journal of chemical physics, 2014. **140**(7): p. 074902.
19. Sugimura, A., et al., *Mechanical properties of a polymer network of Tetra-PEG gel.* Polymer journal, 2013. **45**(3): p. 300-306.
20. Rao, I. and K. Rajagopal, *A study of strain-induced crystallization of polymers.* International Journal of Solids and Structures, 2001. **38**(6): p. 1149-1167.
21. Waheed, N., M. Ko, and G. Rutledge, *Molecular simulation of crystal growth in long alkanes.* Polymer, 2005. **46**(20): p. 8689-8702.
22. Waheed, N., M. Lavine, and G. Rutledge, *Molecular simulation of crystal growth in n-eicosane.* The Journal of chemical physics, 2002. **116**(5): p. 2301-2309.
23. Yi, P. and G.C. Rutledge, *Molecular simulation of crystal nucleation in n-octane melts.* The Journal of chemical physics, 2009. **131**(13): p. 134902.
24. Yi, P. and G.C. Rutledge, *Molecular simulation of bundle-like crystal nucleation from n-eicosane melts.* The Journal of chemical physics, 2011. **135**(2): p. 024903.
25. Lavine, M.S., N. Waheed, and G.C. Rutledge, *Molecular dynamics simulation of orientation and crystallization of polyethylene during uniaxial extension.* Polymer, 2003. **44**(5): p. 1771-1779.
26. Yi, P., C.R. Locker, and G.C. Rutledge, *Molecular dynamics simulation of homogeneous crystal nucleation in polyethylene.* Macromolecules, 2013. **46**(11): p. 4723-4733.
27. Plimpton, S., R. Pollock, and M. Stevens. *Particle-Mesh Ewald and rRESPA for Parallel Molecular Dynamics Simulations*. in *PPSC*. 1997. Citeseer.
28. Nosé, S., *A molecular dynamics method for simulations in the canonical ensemble.* Molecular physics, 1984. **52**(2): p. 255-268.
29. Nosé, S. and M. Klein, *Constant pressure molecular dynamics for molecular systems.* Molecular Physics, 1983. **50**(5): p. 1055-1076.
30. Tsai, J.-L. and J.-F. Tu, *Characterizing mechanical properties of graphite using molecular dynamics simulation.* Materials & Design, 2010. **31**(1): p. 194-199.

31. Hossain, D., et al., *Molecular dynamics simulations of deformation mechanisms of amorphous polyethylene.* Polymer, 2010. **51**(25): p. 6071-6083.

32. Qi, Z., D.K. Campbell, and H.S. Park, *Atomistic simulations of tension-induced large deformation and stretchability in graphene kirigami.* Physical Review B, 2014. **90**(24): p. 245437.

33. Stubbs, J.M., J.J. Potoff, and J.I. Siepmann, *Transferable Potentials for Phase Equilibria. 6. United-Atom Description for Ethers, Glycols, Ketones, and Aldehydes.* The Journal of Physical Chemistry B, 2004. **108**(45): p. 17596-17605.

34. Maerzke, K.A., et al., *TraPPE-UA force field for acrylates and Monte Carlo simulations for their mixtures with alkanes and alcohols.* The Journal of Physical Chemistry B, 2009. **113**(18): p. 6415-6425.

35. Andersen, H.C., *RATTLE: A "Velocity" version of the SHAKE algorithm for molecular dynamics calculations.* Journal of Computational Physics, 1983. **52**(1): p. 24-34.

36. Nguyen, T.D., et al., *Rigid body constraints realized in massively-parallel molecular dynamics on graphics processing units.* Computer Physics Communications, 2011. **182**(11): p. 2307-2313.

37. Paul, W., D.Y. Yoon, and G.D. Smith, *An optimized united atom model for simulations of polymethylene melts.* The Journal of chemical physics, 1995. **103**(4): p. 1702-1709.

38. Hong, B., F. Escobedo, and A.Z. Panagiotopoulos, *Diffusivities and Viscosities of Poly (ethylene oxide) Oligomers†.* Journal of Chemical & Engineering Data, 2010. **55**(10): p. 4273-4280.

39. Fischer, J., et al., *Modeling of aqueous poly (oxyethylene) solutions: 1. Atomistic simulations.* The Journal of Physical Chemistry B, 2008. **112**(8): p. 2388-2398.

40. Bedrov, D., et al., *Simulation and QENS studies of molecular dynamics in aqueous solutions of 1, 2-dimethoxyethane.* The Journal of Physical Chemistry B, 2000. **104**(21): p. 5151-5154.

41. Martin, M.G. and J.I. Siepmann, *Novel Configurational-Bias Monte Carlo Method for Branched Molecules. Transferable Potentials for Phase Equilibria. 2. United-Atom Description of Branched Alkanes.* The Journal of Physical Chemistry B, 1999. **103**(21): p. 4508-4517.

42. Hong, B., A. Chremos, and A.Z. Panagiotopoulos, *Dynamics in coarse-grained models for oligomer-grafted silica nanoparticles.* The Journal of chemical physics, 2012. **136**(20): p. 204904.

43. Takahashi, Y. and H. Tadokoro, *Structural studies of polyethers,(-(CH2) mO-) n. X. Crystal structure of poly (ethylene oxide).* Macromolecules, 1973. **6**(5): p. 672-675.

44. Murthy, N.S., J.R. Knox, and E.T. Samulski, *Order parameter measurements in polypeptide liquid crystals.* The Journal of Chemical Physics, 1976. **65**(11): p. 4835-4839.

45. Flory, P. and A. Vrij, *Melting points of linear-chain homologs. The normal paraffin hydrocarbons.* Journal of the American Chemical Society, 1963. **85**(22): p. 3548-3553.

46. Stehling, F.C. and L. Mandelkern, *The glass temperature of linear polyethylene.* Macromolecules, 1970. **3**(2): p. 242-252.

47. Kavassalis, T. and P. Sundararajan, *A molecular-dynamics study of polyethylene crystallization.* Macromolecules, 1993. **26**(16): p. 4144-4150.

48. Luo, X., et al., *The relationship between the degree of branching and glass transition temperature of branched polyethylene: experiment and simulation.* Polymer Chemistry, 2014. **5**(4): p. 1305-1312.

49. Wick, C.D., M.G. Martin, and J.I. Siepmann, *Transferable potentials for phase equilibria. 4. United-atom description of linear and branched alkenes and alkylbenzenes.* The Journal of Physical Chemistry B, 2000. **104**(33): p. 8008-8016.

50. Kennedy, M., A. Peacock, and L. Mandelkern, *Tensile properties of crystalline polymers: linear polyethylene.* Macromolecules, 1994. **27**(19): p. 5297-5310.

51. Flory, P.J., *Thermodynamics of crystallization in high polymers. I. Crystallization induced by stretching.* The Journal of Chemical Physics, 1947. **15**(6): p. 397-408.

52. Schaerer, A., et al., *Properties of pure normal alkanes in the C17 to C36 range.* Journal of the American Chemical Society, 1955. **77**(7): p. 2017-2019.

53. Hwo, C.H. and J.F. Johnson, *Determination of young's modulus of elastomers by use of a thermomechanical analyzer.* Journal of Applied Polymer Science, 1974. **18**(5): p. 1433-1441.

54. Alexandre, M., et al., *Preparation and properties of layered silicate nanocomposites based on ethylene vinyl acetate copolymers.* Macromolecular rapid communications, 2001. **22**(8): p. 643-646.

55. Andreopoulos, A. and E. Kampouris, *Mechanical properties of crosslinked polyethylene.* Journal of applied polymer science, 1986. **31**(4): p. 1061-1068.

56. Nakafuku, C. and M. Sakoda, *Melting and crystallization of poly (L-lactic acid) and poly (ethylene oxide) binary mixture.* Polymer journal, 1993. **25**(9): p. 909-917.

57. Satterfield, M.B., et al., *Mechanical properties of Nafion and titania/Nafion composite membranes for polymer electrolyte membrane fuel cells.* Journal of Polymer Science Part B: Polymer Physics, 2006. **44**(16): p. 2327-2345.

58. Dalton, A.B., et al., *Super-tough carbon-nanotube fibres.* Nature, 2003. **423**(6941): p. 703-703.

59. Vollrath, F. and D.P. Knight, *Liquid crystalline spinning of spider silk.* Nature, 2001. **410**(6828): p. 541-548.

60. Saraf, R.F. and R.S. Porter, *Deformation of semicrystalline polymers via crystal–crystal phase transition.* Journal of Polymer Science Part B: Polymer Physics, 1988. **26**(5): p. 1049-1057.

61. Schwenke, K., M. Lang, and J.-U. Sommer, *On the Structure of Star–Polymer Networks.* Macromolecules, 2011. **44**(23): p. 9464-9472.

62. Matsunaga, T., et al., *SANS and SLS studies on tetra-arm PEG gels in as-prepared and swollen states.* Macromolecules, 2009. **42**(16): p. 6245-6252.

63. Lange, F., et al., *Connectivity and structural defects in model hydrogels: A combined proton NMR and Monte Carlo simulation study.* Macromolecules, 2011. **44**(24): p. 9666-9674.

64. Burbank, S.D. and L.V. Smith, *Dynamic characterization of rigid foam used in finite element sports ball simulations.* Proceedings of the Institution of Mechanical Engineers, Part P: Journal of Sports Engineering and Technology, 2012: p. 1754337112441112.

65. Vollenberg, P. and D. Heikens, *Particle size dependence of the Young's modulus of filled polymers: 1. Preliminary experiments.* Polymer, 1989. **30**(9): p. 1656-1662.

Supplemental Information

Table S1 Lennard-Jones Potential for Tetra-PE systems.

	ε (kJ/mol)	σ (nm)
CH_2	0.3825	0.395
C	0.004157	0.640

Table S2 Lennard-Jones Potential for Tetra-PEG systems.

	ε (kJ/mol)	σ (nm)
C	0.004157	0.640
CH_2	0.3825	0.395
CH3	0.8148	0.375
O	0.4593	0.280

Table S3 Dihedral parameters in the Modified TraPPE-UA force field.

	k_i(kJ/mol)							
	i = 0	1	2	3	4	5	6	7
CH_x-O-CH_y-CH_y	-0.2539	-5.15997	-0.69711	5.35013	0.80312	0.28307	0.09526	-0.05797
O-CH_x-CH_x-O	-7.75967	7.58526	6.70523	8.40071	0.63221	0.11063	0.35962	0.01683

Table S4 Dihedral parameters for crosslinks.

	k_i(kJ/mol)			
	i = 1	2	3	4
O-CH_2-C-CH_2	12.28832	-0.88701	12.80304	0
C-CH_2-O-CH_2	12.06164	-2.72295	9.282204	0

Table S5 Validation of modified TraPPE-UA force field using mean squared end-to-end distance $\langle r^2 \rangle$ of the PEO chains.

		Published Results		Simulations Results	
PEO (n)	number of chains	ρ (g/cm^3)	<r^2> (nm^2)	ρ (g/cm^3)	<r^2> (nm^2)
n=5	N=50	1.016	1.724	1.014	1.691
n=9	N=150	1.056	3.419	1.056	3.396

Table S6 The Young's moduli of Tetra-PE systems and different polymer materials (a: [64], b: [54] and c: [53]).

Number of CH_2 Unit	Molecular Weight of Network Strand	Young's Modulus (GPa)	Comparing Polymer Materials	Young's Modulus (GPa)
6	85	0.191	Rigid Polymer Foam (HD)	0.138 [a]
12	170	0.0762		
18	255	0.0492	Silicone Elastomers	0.011 [b]
30	425	0.0261		
39	553	0.0254	Ethylene-Vinyl Acetate (EVA)	0.012 [c]
75	1063	0.0122		
100	1417	0.0116		

Table S7 The Young's moduli of Tetra-PEG systems and different polymer materials (a: [65], b: [57]).

Number of CH_2CH_2O Unit	Molecular Weight of Network Strand	Young's Modulus (Gpa)	Polymer Materials	Young's Modulus (GPa)
1	88	1.613	Polyethylene	1.56 [a]
3	176	0.437		
5	264	0.36		
9	440	0.238		
12	572	0.212	Ionomer Nafion	0.1 [b]
24	1100	0.151		
40	1804	0.141		

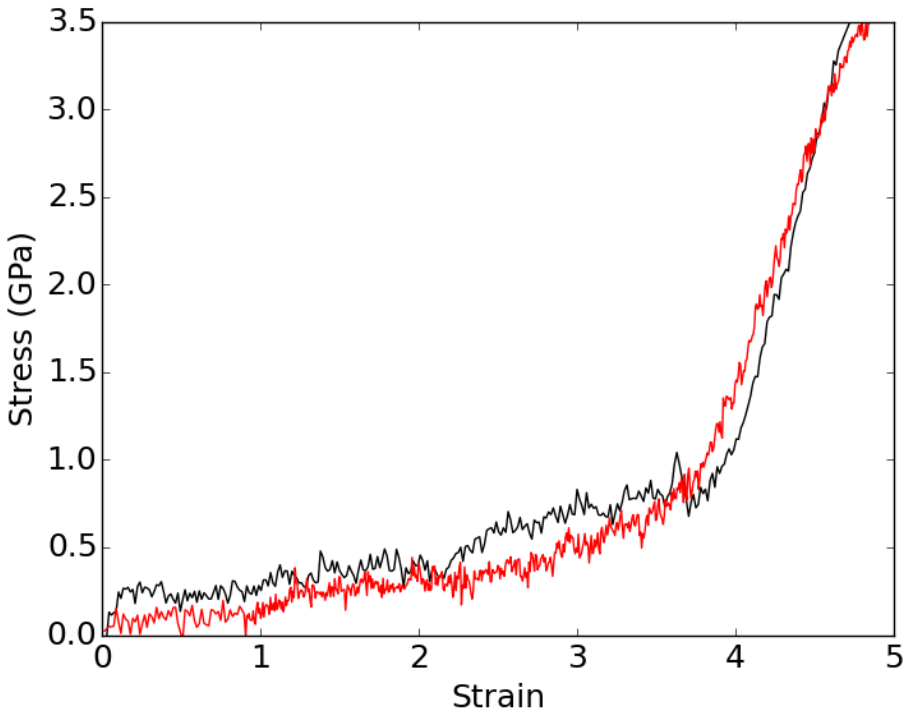

Figure S1 Stress-strain curves obtained from uniaxial deformation simulations of an n=9 Tetra-PEG amorphous network using (i) strain-driven ensemble at T = 303 K (black line), and (ii) stress-driven ensemble at T = 303 K, $P_{xx} = P_{yy} = 1$ bar (red line).

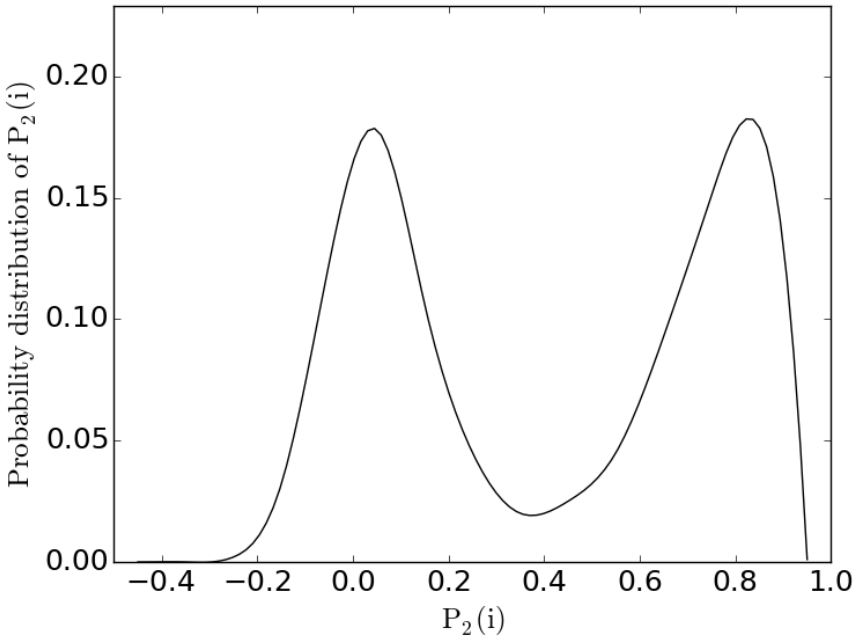

Figure S2 Local order $P_2(i)$ probability distribution for the n-eicosane system with a half-crystal, half-melt configuration. The bimodal distribution calculated based on the protocols and parameter values described by Yi and Rutledge [24] correctly capture the physical state of the system.

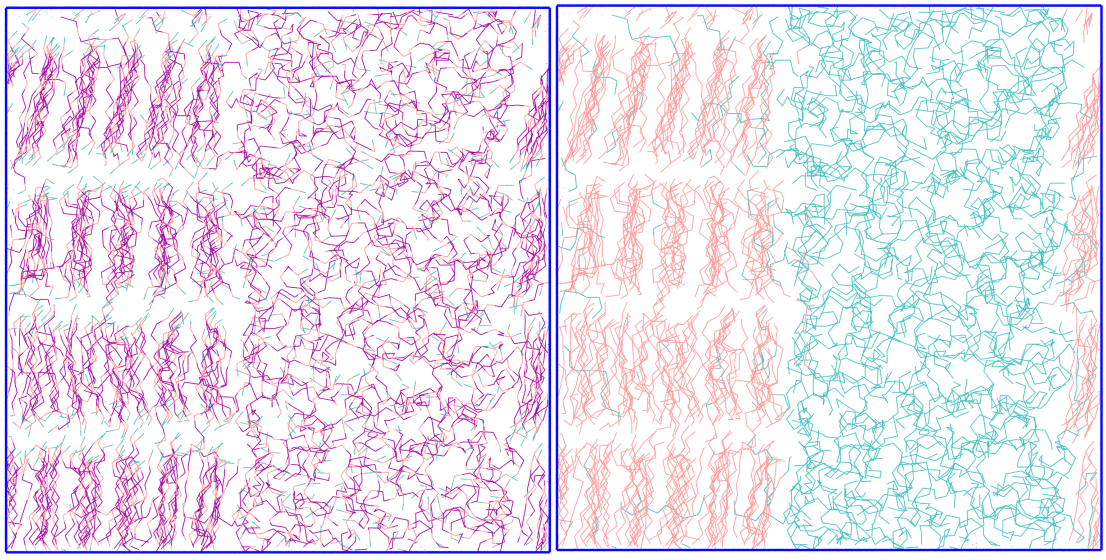

Figure S3 Left: a half-crystal, half-melt n=3 PEO system having 576 PEO molecules, with the crystal region formed at T = 276 K and P = 1 atm, and the amorphous region was relaxed at T = 500 K, P = 1 atm. Right: the crystal (pink) and amorphous (cyan) regions are clearly discerned from each other by using the modified local order parameter, with degree of coarse-graining d = 6.

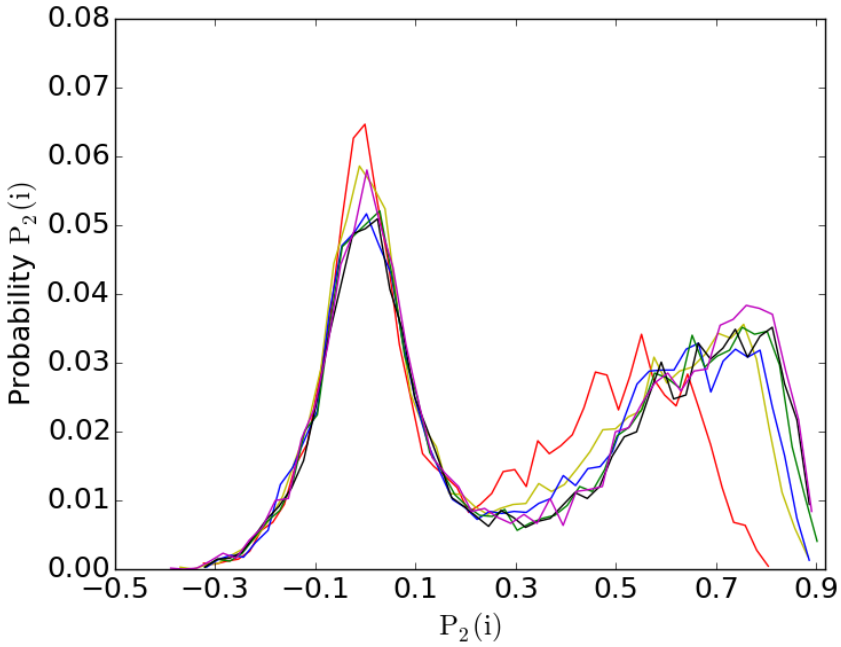

Figure S4 Probability distribution of n=3 PEO system with a half-crystal, half-melt state using a modified local order parameter $P_2(i)$, with degree of coarse-graining d = 3 (red), 4 (yellow), 5 (blue), 6 (green), 7 (black) and 8 (magenta).

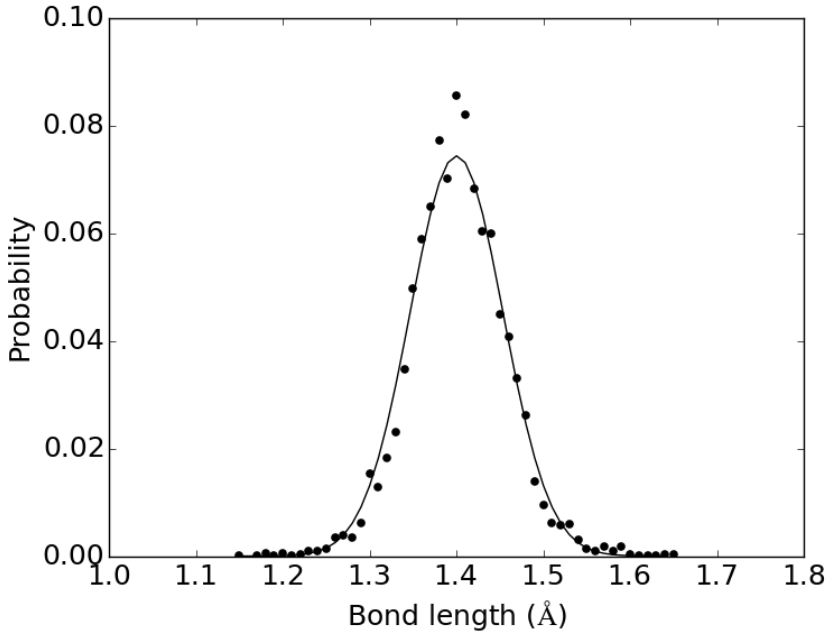

Figure S5 Probability distribution of CH_x-CH_x bond length of the n=100 Tetra-PE diamond network equilibrated at T = 303 K and P = 1 atm; the results were obtained by averaging 10 simulation configurations collected 10, 000 fs apart.

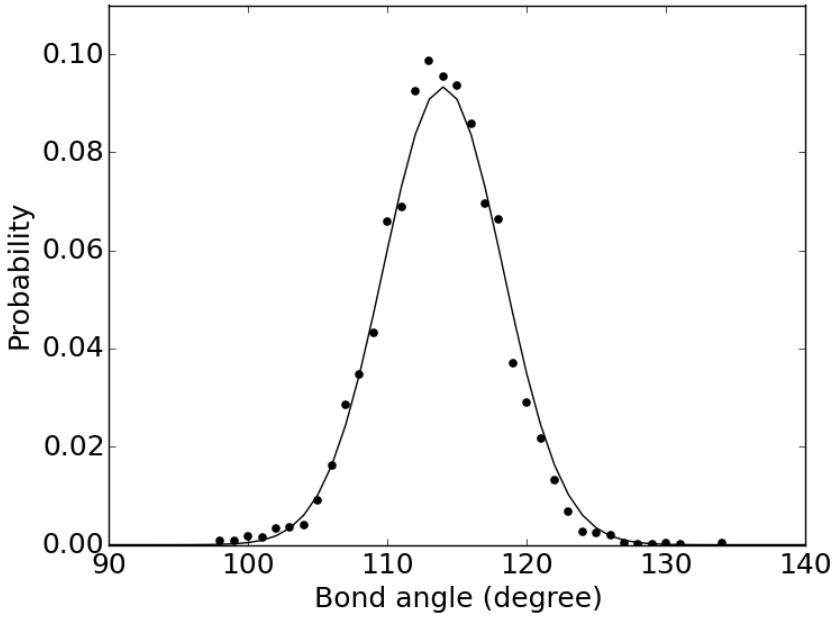

Figure S6 CH_2-C-CH_2 angle probability distribution of the n=100 Tetra-PE diamond network equilibrated at 303 K and P = 1 atm; the results were obtained by averaging 10 simulation configurations collected 10, 000 fs apart.

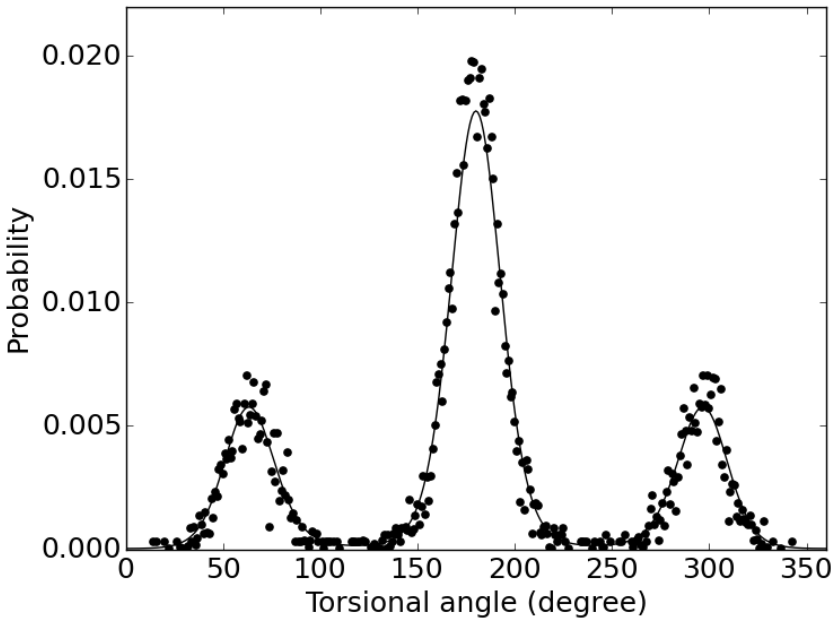

Figure S7 CH_x-CH_x-CH_x-CH_x torsional angle probability distribution of the n=100 Tetra-PE diamond network equilibrated at 303 K and P = 1 atm; the results were obtained by averaging 10 simulation configurations collected 10, 000 fs apart.

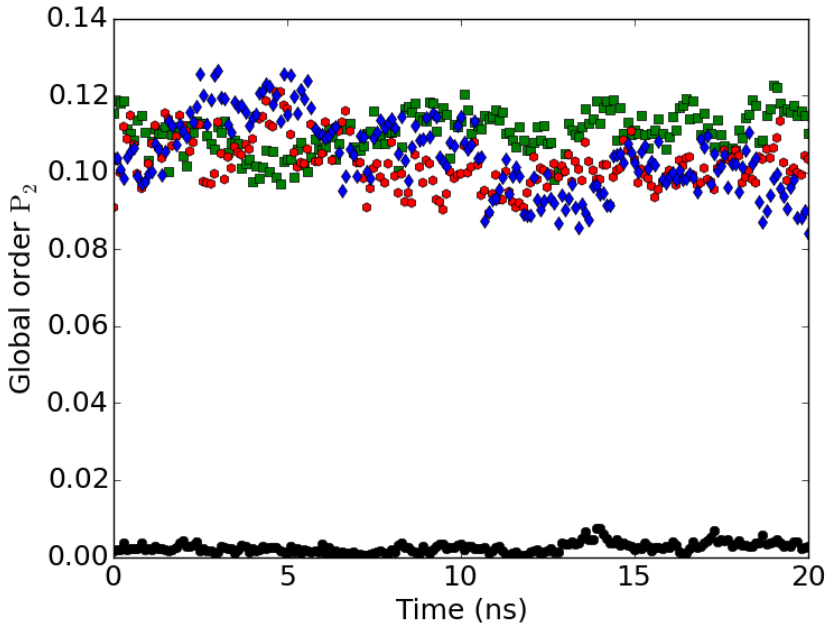

Figure S8 Global order parameter of the n=100 Tetra-PE diamond network equilibrated at different temperatures [P = 1 atm, T = 300 K (green), 310 K (red), 315 K (blue), 320 K (black)].

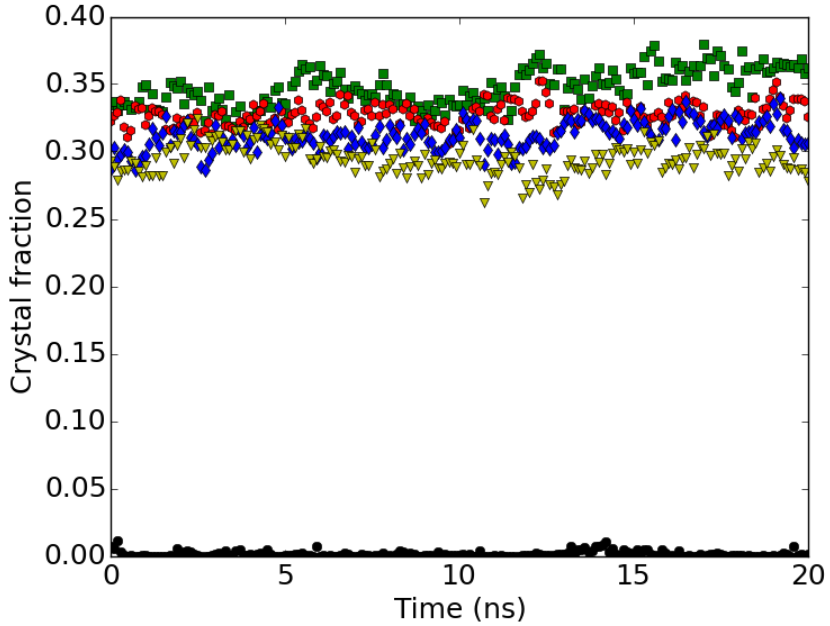

Figure S9 Crystal fraction of the Tetra-PE (n=100) diamond network at various temperatures [P = 1 atm. T = 280 K (green), 300 K (red), 310 K (blue), 315 K (yellow), 320 K (black)]. The calculation was based on the local order parameter method.

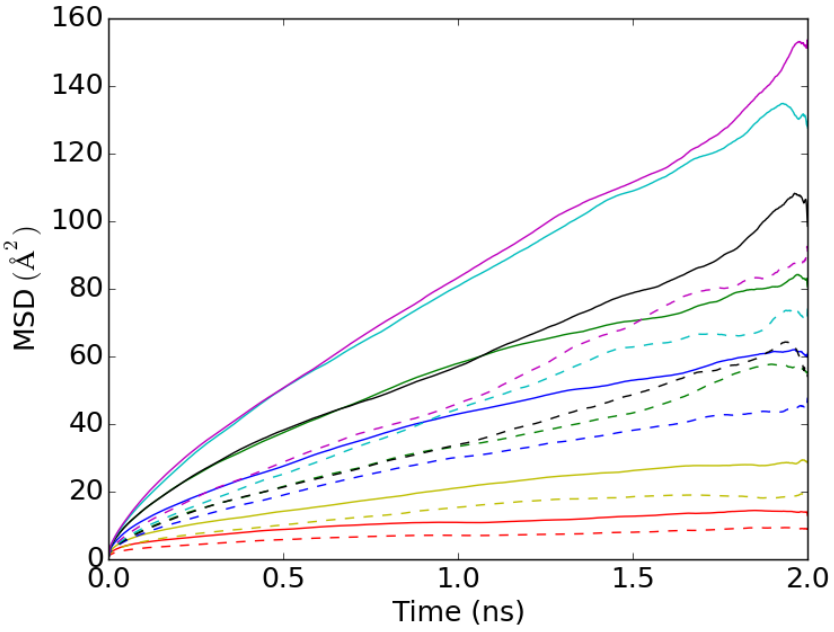

Figure S10 Mean-squared-displacement of the middle atoms of the network strands (solid line) and of the crosslinks (dashed line) of amorphous Tetra-PE diamond networks equilibrated at T = 260 K, P = 1 atm, with degree of polymerization n=6 (red), 12 (yellow), 18 (blue), 30 (green), 39 (black), 75 (cyan) and 100 (magenta).

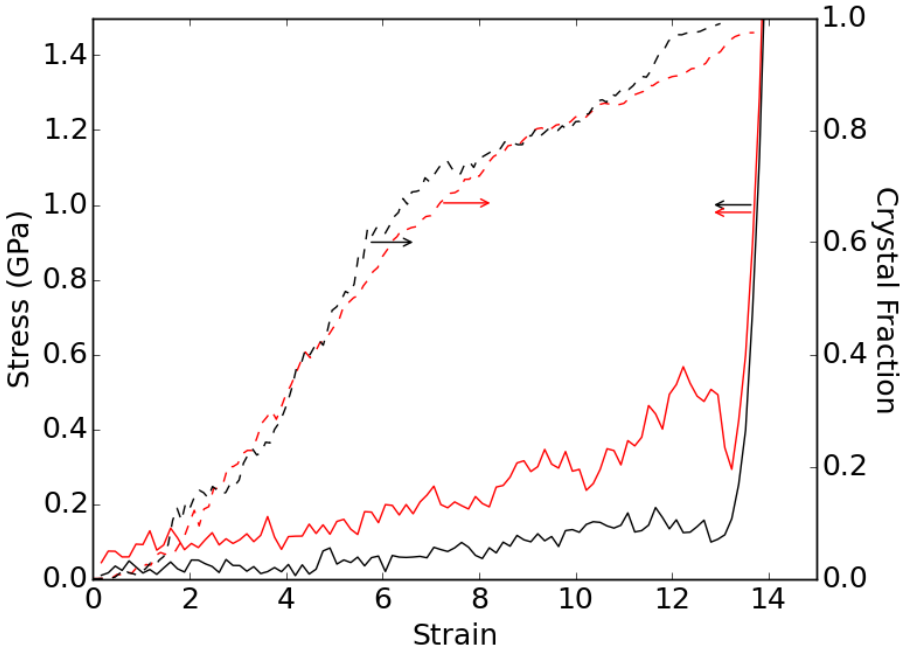

Figure S11 Stress-strain and crystal fraction vs. strain from uniaxial deformation simulations of the n=100 Tetra-PE diamond network using an NVT ensemble at T = 303 K and strain rate of $\dot{r} = 2.5\times10^{-5}$ fs^{-1}(red) and $\dot{r} = 2.5\times10^{-6}$ fs^{-1}(black).

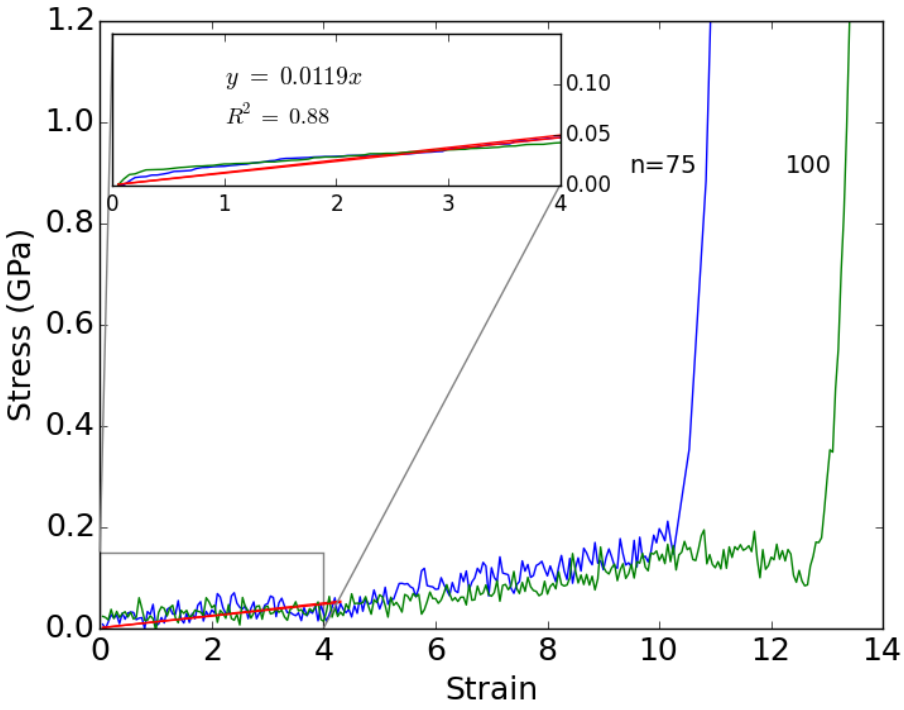

Figure S12 Estimation of the Young's modulus from a linear fit of the low-strain regime of the stress-strain curves for n=75 and 100 Tetra-PE diamond networks; the slope of the fitting line (red) corresponds to a Young's modulus of $E = 0.012 \pm 0.005$ GPa. The inset shows the low strain region after using a digital filter to eliminate high-frequency noise.

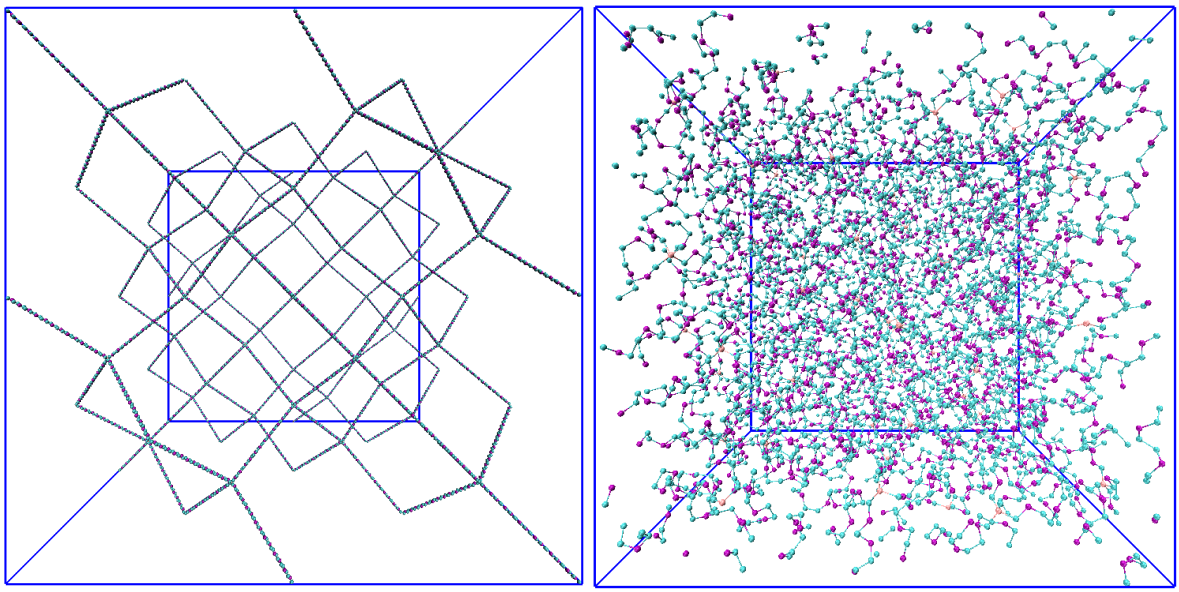

Figure S13 Left: the initial fully extended configuration of the n=5 Tetra-PEG diamond network. Right: the same system upon collapsing into a high-density amorphous melt in a 2 ns simulation at T = 303 K, P = 1 atm.

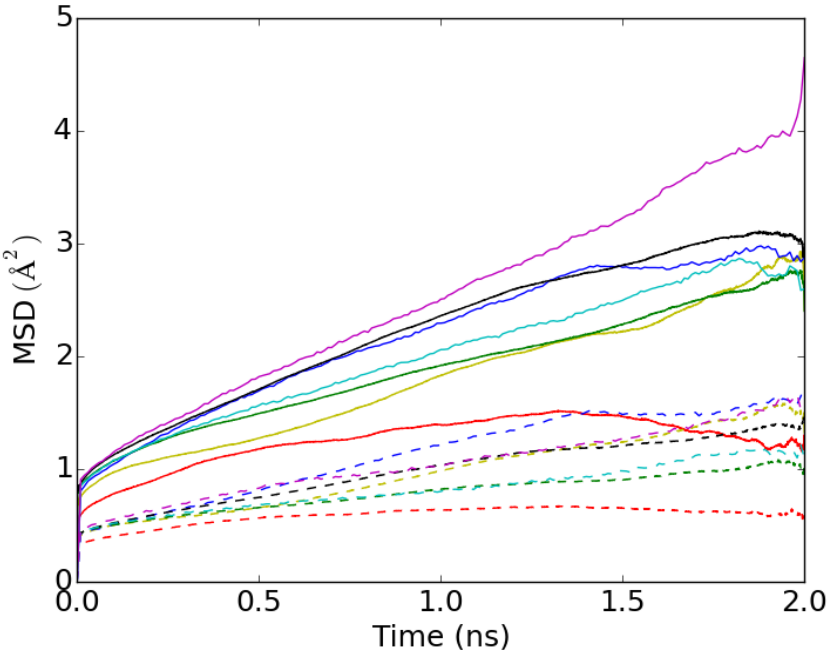

Figure S14 Mean-squared-displacement of the middle atoms of the network strands (solid line) and of the crosslinks (dashed line) of amorphous Tetra-PEG diamond networks equilibrated at T = 260 K, P = 1 atm, with degree of polymerization n=1 (red), 3 (yellow), 5 (green), 9 (cyan), 12 (blue), 24 (black) and 40 (magenta).

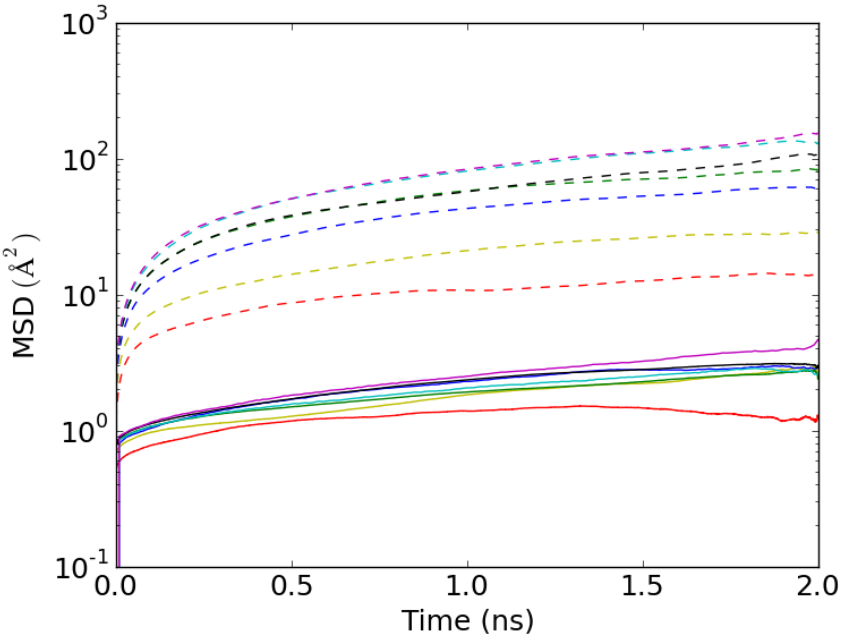

Figure S15 Mean-squared-displacement of the middle atoms of the network strands of amorphous Tetra-PE (dash lines) [with n=6 (red), 12 (yellow), 18 (blue), 30 (green), 39 (black), 75 (cyan) and 100 (magenta)] and Tetra-PEG networks (solid lines) [with n=1 (red), 3 (yellow), 5 (green), 9 (cyan), 12 (blue), 24 (black) and 40 (magenta)] equilibrated at T = 260 K, P = 1 atm.

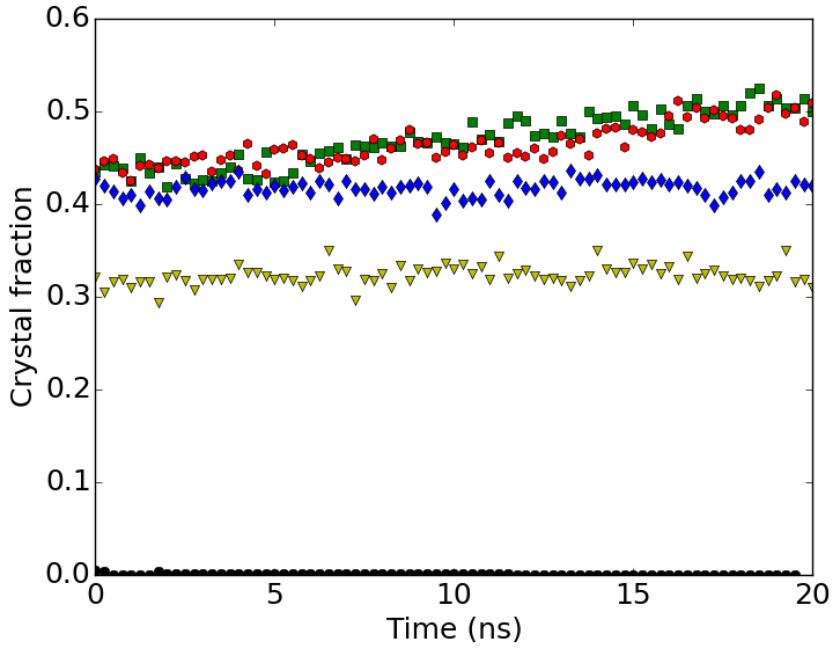

Figure S16 The crystal fraction of 100 PEO (n=30) chains at various temperatures [P = 1 atm. T = 320 K (green), 330 K (red), 340 K (blue), 350 K (yellow), 360 K (black)]. The calculation was based on the modified local order parameter.

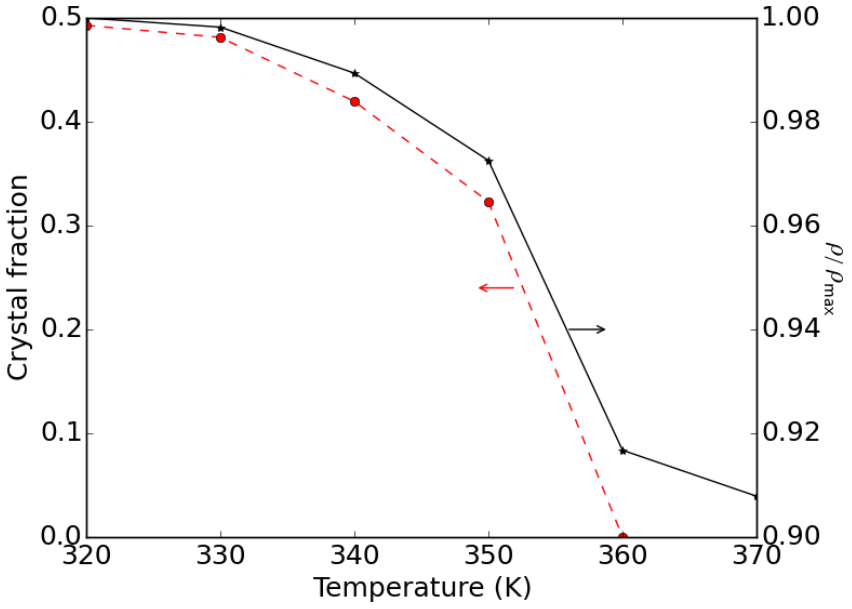

Figure S17 Normalized density and crystal fraction of 100 PEO (n=30) molecules equilibrated at different temperatures.

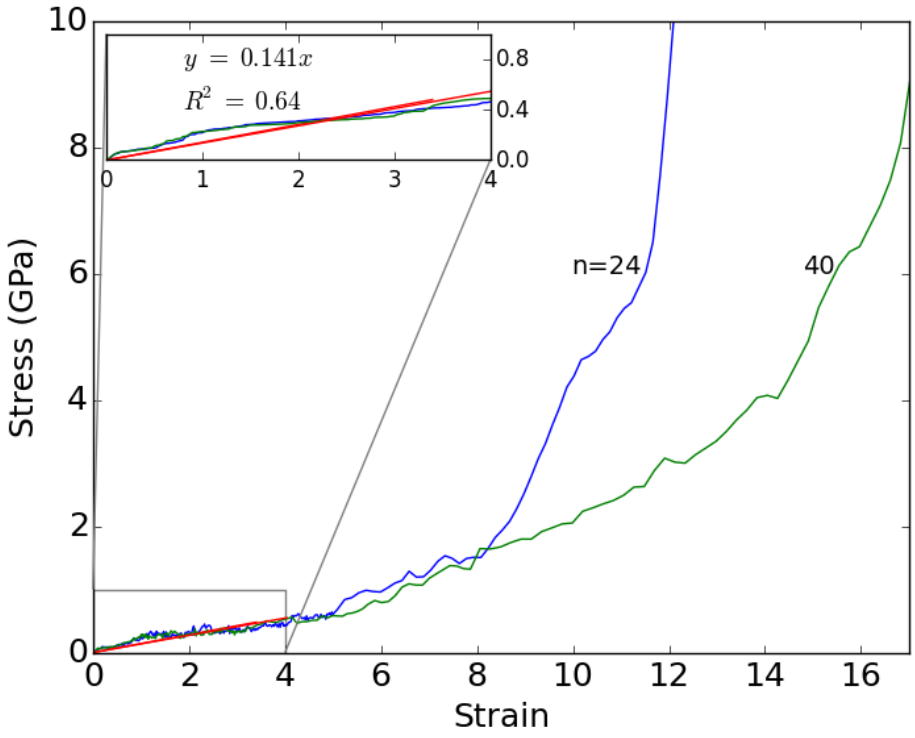

Figure S18 Estimation of the Young's modulus by a linear fit of the low-strain regime of the stress-strain curves for n=24 and 40 Tetra-PEG diamond networks; the slope of the fitting line (red) corresponds to a Young's modulus of $E = 0.14 \pm 0.05$ GPa. The inset shows the low strain region after using a digital filter to eliminate high-frequency noise.